JACS JOURNAL OF THE AMERICAN CHEMICAL SOCIETY

Article

Cite This: J. Am. Chem. Soc. 2019, 141, 11700−11712

pubs.acs.org/JACS

Room Temperature Acceptorless Alkane Dehydrogenation from Molecular σ-Alkane Complexes

Alasdair I. McKay,[†,§] Alexander J. Bukvic,[†,§] Bengt E. Tegner,[‡,§] Arron L. Burnage,[‡] Antonio J. Martínez-Martínez,[†] Nicholas H. Rees,[†] Stuart A. Macgregor,*[,‡] and Andrew S. Weller*[,†]

[†]Chemistry Research Laboratories, University of Oxford, Oxford OX1 3TA, United Kingdom

[‡]Institute of Chemical Sciences, Heriot Watt University, Edinburgh EH14 4AS, United Kingdom

Supporting Information

ABSTRACT: The non-oxidative catalytic dehydrogenation of light alkanes via C−H activation is a highly endothermic process that generally requires high temperatures and/or a sacrificial hydrogen acceptor to overcome unfavorable thermodynamics. This is complicated by alkanes being such poor ligands, meaning that binding at metal centers prior to C−H activation is disfavored. We demonstrate that by biasing the pre-equilibrium of alkane binding, by using solid-state molecular organometallic chemistry (SMOM-chem), well-defined isobutane and cyclohexane σ-complexes, [Rh(Cy$_2$PCH$_2$CH$_2$PCy$_2$)(η:η-(H$_3$C)CH(CH$_3$)$_2$][BAr$^F_4$] and [Rh(Cy$_2$PCH$_2$CH$_2$PCy$_2$)(η:η-C$_6$H$_{12}$)][BAr$^F_4$] can be prepared by simple hydrogenation in a solid/gas single-crystal to single-crystal transformation of precursor alkene complexes. Solid-gas H/D exchange with D$_2$ occurs at all C−H bonds in both alkane complexes, pointing to a variety of low energy fluxional processes that occur for the bound alkane ligands in the solid-state. These are probed by variable temperature solid-state nuclear magnetic resonance experiments and periodic density functional theory (DFT) calculations. These alkane σ-complexes undergo spontaneous acceptorless dehydrogenation at 298 K to reform the corresponding isobutene and cyclohexadiene complexes, by simple application of vacuum or Ar-flow to remove H$_2$. These processes can be followed temporally, and modeled using classical chemical, or Johnson−Mehl−Avrami−Kologoromov, kinetics. When per-deuteration is coupled with dehydrogenation of cyclohexane to cyclohexadiene, this allows for two successive KIEs to be determined [k_H/k_D = 3.6(5) and 10.8(6)], showing that the rate-determining steps involve C−H activation. Periodic DFT calculations predict overall barriers of 20.6 and 24.4 kcal/mol for the two dehydrogenation steps, in good agreement with the values determined experimentally. The calculations also identify significant C−H bond elongation in both rate-limiting transition states and suggest that the large k_H/k_D for the second dehydrogenation results from a pre-equilibrium involving C−H oxidative cleavage and a subsequent rate-limiting β-H transfer step.

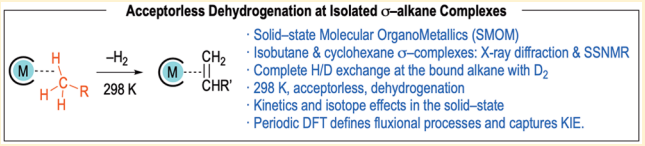

INTRODUCTION

The "on-purpose" non-oxidative catalytic dehydrogenation of abundant, unreactive and low value light alkanes to produce alkenes, which are key chemical intermediates, is of significant industrial importance,[1,2] and is amplified by the recent movement in feedstocks from naphtha to shale gas. Dehydrogenation is an energy intensive process, due to the high positive enthalpy of reaction (e.g., isobutane, cyclohexane: $\Delta H_r^\circ \sim 118$ kJmol^{-1}, Scheme 1A),[3] and high temperatures are thus required to drive the reaction (commonly 550−750 °C using a heterogeneous catalyst), which present challenges for catalyst decomposition, coking and process selectivity.[4] In molecular homogeneous dehydrogenation systems a sacrificial alkene H$_2$-acceptor is commonly used at operating temperatures of 120−200 °C,[5−7] or lower with more exotic acceptors.[8] In the absence of an acceptor dehydrogenation can be driven photolytically,[9−11] or by continuous removal of H$_2$ at elevated temperatures (∼150 °C) to bias the thermodynamics.[12−14]

Key, but undetected, first-formed intermediates in both homogeneously and heterogeneously catalyzed alkane dehydrogenation are σ-alkane complexes, in which the C−H bond of an alkane interacts with the metal center, in a 3-center 2-electron σ-interaction, prior to C−H oxidative bond cleavage and β-hydrogen elimination (Scheme 1B).[15−18] As C−H bonds in alkanes are strong, non-polar and relatively sterically crowded, alkanes are very poor ligands (M···H−C bond enthalpies less than 60 kJ mol^{-1}), meaning that such complexes have generally only been observed using low temperature in situ (−80 °C or lower) nuclear magnetic resonance (NMR)[19−22] or in situ diffraction techniques,[23] or on very short timescales (μs to s) using time resolved infrared experiments (TRIR).[24−26] An additional challenge for catalytic alkane dehydrogenation is thus one of pre-equilibrium prior to C−H activation, as solvent or other ligands will generally outcompete any weak σ-interaction from the alkane under normal conditions.[21,27−31] However, C−H activation can be a rather facile process once a σ-complex is formed.[7,26,32−34] Combined, all these factors make observing intermolecular

Received: May 24, 2019
Published: June 27, 2019

Scheme 1. (A) Nonoxidative Dehydrogenation of Cyclohexane and Isobutane; (B) σ-Alkane Complexes: Pre-equilibrium, C−H Oxidative Cleavage and Dehydrogenation[a]

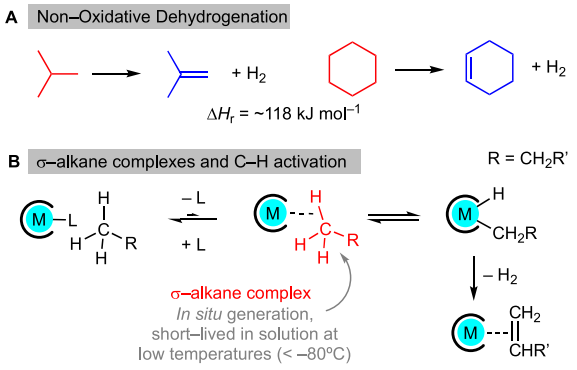

[a]L = ligand or solvent.

Scheme 2. SMOM Approach to the Synthesis of Stable σ-Alkane Complexes in the Solid-State

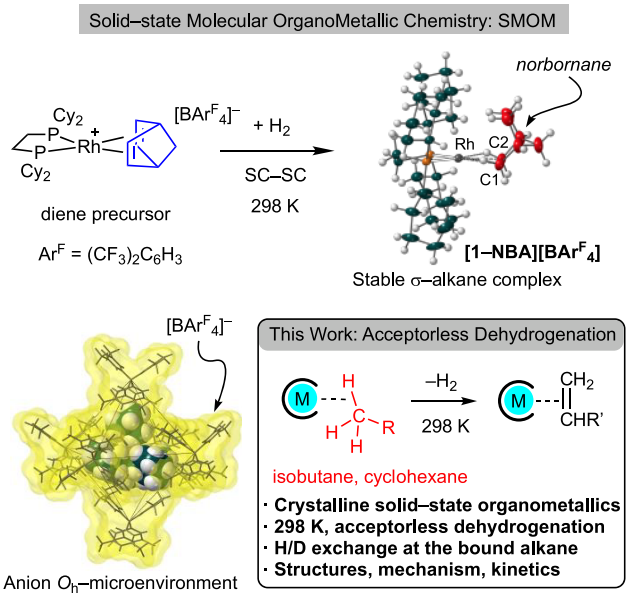

dehydrogenation processes directly from σ-alkane complexes very challenging, and many experimental contributions have thus focused on the overall thermodynamics and catalytic efficiencies of such processes, as well as kinetic studies of catalytic systems, including isotopic substitution.[5,35] Such work has also been supported by numerous computational studies.[25,36,37]

We have recently reported that σ-alkane complexes can be prepared using so-called solid-state molecular organometallic (SMOM) chemistry techniques. By operating under single-crystal to single-crystal conditions (SC-SC),[38] addition of H_2 to precursor norbornadiene complexes, e.g., [Rh($R_2PCH_2CH_2PR_2$)($\eta^2\eta^2$-C_7H_8)][BAr^F_4] (R = ^{i}Pr, Cy, Cyp; Ar^F = 3,5-$(CF_3)_2C_6H_3$) generates the corresponding σ-alkane (i.e., norbornane) complexes directly in the solid-state. Some of these show remarkable stability at room temperature, which we postulate is due to the, albeit non-porous, octahedral nanoreactor[39] environment provided by the [BAr^F_4]$^-$ anions (Scheme 2, R = Cy, [**1-NBA**][$\mathbf{BAr^F_4}$]).[40−43]

We now report that by using this methodology the synthesis of σ-complexes of the light alkanes cyclohexane and isobutane can be achieved at Rh(I) centers, which allow for their detailed characterization by single-crystal X-ray diffraction, solid-state NMR (SSNMR) spectroscopy and periodic density functional theory (DFT) calculations. These complexes are shown to undergo rapid H/D exchange at all the C−H bonds of the bound alkane on addition of D_2, and a remarkable acceptorless dehydrogenation at 25 °C by simple removal of H_2 under flow or vacuum, for which significant kinetic isotope effects can be directly measured for the dehydrogenation of cyclohexane. The products of dehydrogenation, cyclohexene and isobutene, are key intermediates in the chemical manufacturing chain (nylon production and gasoline additives/butyl rubber respectively).[44,45] In particular, isobutene is currently produced commercially using a high temperature non-oxidative dehydrogenation of isobutane (e.g., the Oleflex process: heterogeneous Pt/Sn catalyst at 525−700 °C). Our results provide definitive structural and reactivity data for the key intermediates in both heterogeneous and homogeneous catalytic dehydrogenation processes. They also demonstrate the potential for SMOM systems to mediate low temperature dehydrogenation by biasing both the pre-equilibrium toward σ-complexes, and the overall dehydrogenation by straightforward removal of H_2.

RESULTS AND DISCUSSION

Synthesis and Characterization of Isobutane and Cyclohexane σ-Alkane Complexes. Alkene precursors to the σ-alkane complexes, namely isobutene [Rh($Cy_2PCH_2CH_2PCy_2$)(C_4H_8)][BAr^F_4] [**1-C_4H_8**][$\mathbf{BAr^F_4}$] and cyclohexadiene [Rh($Cy_2PCH_2CH_2PCy_2$)(η^4-C_6H_8)][BAr^F_4] [**1-C_6H_8**][$\mathbf{BAr^F_4}$] were prepared in good yield as crystalline materials (Figure 1A).[46] While [**1-C_6H_8**][$\mathbf{BAr^F_4}$] is prepared using traditional solution routes, [**1-C_4H_8**][$\mathbf{BAr^F_4}$] is best accessed via SC-SC solid/gas reactivity by addition of gaseous isobutene to [**1-NBA**][$\mathbf{BAr^F_4}$] and displacement of NBA,[47] followed by recrystallization from a solution saturated with isobutene. Single crystal X-ray diffraction, low temperature solution and SSNMR spectroscopy confirm the formulations as alkene complexes.[46] The solid-state structure of the isobutene complex [**1-C_4H_8**][$\mathbf{BAr^F_4}$] has a bound alkene fragment that also has an additional supporting agostic Rh···H_3C interaction, and so features an $\eta^2\pi$:η^2_{C-H}-binding mode, similar to the recently reported propene analogue.[47] The isobutene is disordered over two superimposed positions that are related by a non-crystallographic apparent C_2 axis, which means that discussion of the detailed bond metrics is not appropriate. The cyclohexadiene complex, [**1-C_6H_8**][$\mathbf{BAr^F_4}$] adopts the expected η^4 diene binding mode (Figure S95). Both [**1-C_4H_8**][$\mathbf{BAr^F_4}$] and [**1-C_6H_8**][$\mathbf{BAr^F_4}$] have extended solid-state structures in which the organometallic cation is surrounded in a pseudo-O_h cavity defined by the [BAr^F_4]$^-$ anions (Figures S93 and S95),[46] and Figure 1C shows this for [**1-C_4H_8**][$\mathbf{BAr^F_4}$]. [**1-C_4H_8**][$\mathbf{BAr^F_4}$] is a rare example of a crystallographically characterized isobutene complex.[48]

Like its propene analogue,[47] the isobutene complex [**1-C_4H_8**][$\mathbf{BAr^F_4}$] exhibits fluxional processes at 298 K in both solution and the solid-state that exchange the methyl and methylene hydrogens. This symmetry in the cation is demonstrated by a single environment being observed in the 298 K $^{31}P\{^1H\}$ NMR solution spectrum [δ 95.3, d, J(RhP) =

DOI: 10.1021/jacs.9b05577
J. Am. Chem. Soc. 2019, 141, 11700−11712

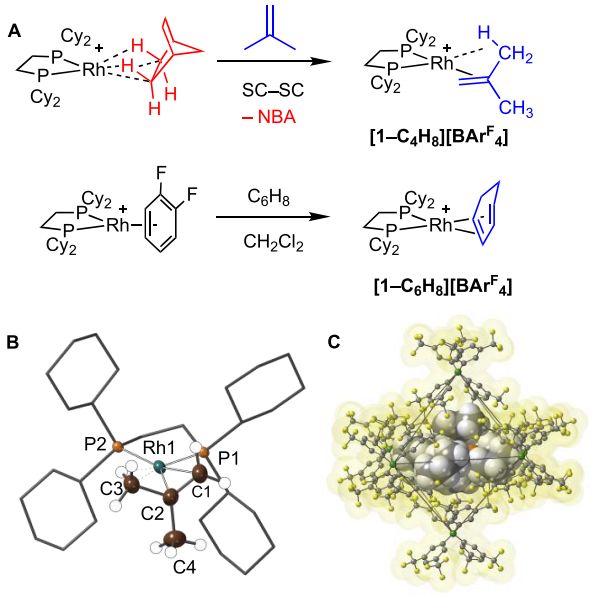

Figure 1. (A) Synthesis of $[\mathbf{1}\text{-}C_4H_8][BAr^F{}_4]$ and $[\mathbf{1}\text{-}C_6H_8][BAr^F{}_4]$. (B) Solid-state structure of $[\mathbf{1}\text{-}C_4H_8][BAr^F{}_4]$. Displacement ellipsoids shown at the 30% probability level. $[BAr^F{}_4]^-$ anions and most hydrogen atoms omitted for clarity. One disordered component shown. Rh1–P1, 2.2238(9); Rh1–P2, 2.2400(9); Rh1–C1, 2.262(6); Rh1–C2, 2.136(8); Rh1–C3, 2.368(9); C1–C2, 1.320(12); C2–C3, 1.474(13), 1.513(13). (C) Packing diagram of $[\mathbf{1}\text{-}C_4H_8][BAr^F{}_4]$ (van der Waals radii) showing the O_h arrangement of $[BAr^F{}_4]^-$ anions.

179 Hz], while no distinct alkene resonances are observed in the $^{13}C\{^1H\}$ NMR (solid-state or solution) or ^1H NMR spectra (solution). We propose a 1,3-shift via an methallyl hydride intermediate,[49] coupled with a further exchange of two methyl groups by libration. These can be slowed at low temperature, i.e., 183 K solution, 158 K solid-state. Thus, in solution two mutually coupled environments are now observed in the low temperature $^{31}P\{^1H\}$ NMR spectrum at δ 97.6 [dd, J(RhP) = 201, J(PP) = 26 Hz], 93.6 [dd, J(RhP) 158, J(PP) = 26 Hz]. The $^{31}P\{^1H\}$ SSNMR spectrum shows two overlapping environments centered at δ 94.8. The solution $^{13}C\{^1H\}$ NMR spectrum shows two signals due to the coordinated alkene [δ 111.5, 72.6], and the ^1H NMR spectrum shows a signal that can be assigned to the alkene groups and an agostic Rh···H_3C interaction [δ −0.15], although the low temperature limit was not reached (Figures S1–7). The $^{13}C\{^1H\}$ SSNMR spectrum shows alkene signals at δ 108.6 and 70.6. The agostic Rh···H_3C signal could not be unambiguously identified, but a resonance at δ 15.7 that is absent in the 298 K spectrum is consistent with such an interaction.[47] In contrast, $[\mathbf{1}\text{-}C_6H_8][BAr^F{}_4]$ does not show any fluxional behavior, and its NMR spectra are unremarkable.

Addition of H_2 (298 K, 1 bar, 15 min) to single-crystalline samples of each of the alkene complexes resulted in rapid hydrogenation of the alkene to form the corresponding σ–alkane complexes, $[\mathbf{1}\text{-}C_4H_{10}][BAr^F{}_4]$ and $[\mathbf{1}\text{-}C_6H_{12}][BAr^F{}_4]$, via SC-SC transformations, Scheme 3A, in which the O_h arrangement of $[BAr^F{}_4]^-$ anions is retained (Figures S94 and S96). Analysis of the isobutane σ-complex $[\mathbf{1}\text{-}C_4H_{10}][BAr^F{}_4]$ by single-crystal X-ray diffraction (R = 9.5%, two independent molecules in the unit cell) shows the Rh(I)-center has two η^2-Rh···H–C interactions[42] from adjacent methyl (C1) and methine (C2) groups in the alkane [e.g., Rh···C1, 2.362(14); Rh···C2, 2.442(7) Å for one of the independent molecules in the unit cell], Figure 2. These distances are similar to those in

Scheme 3. Synthesis and Stability of $[\mathbf{1}\text{-}C_4H_{10}][BAr^F{}_4]$ and $[\mathbf{1}\text{-}C_6H_{12}][BAr^F{}_4]$

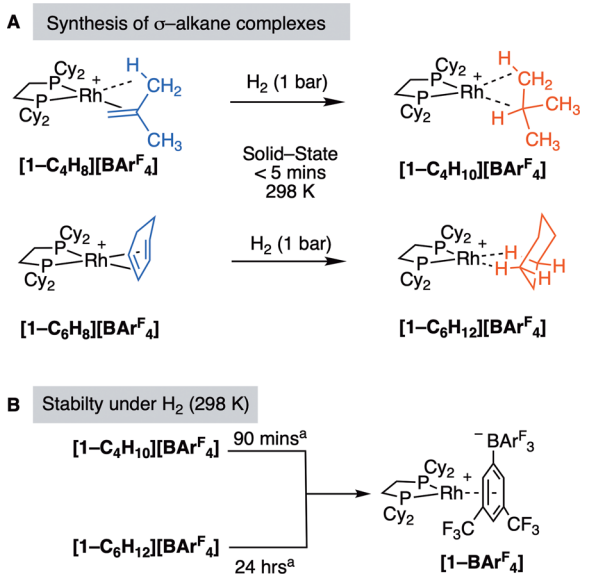

[a]Time for ~10% decomposition in the solid-state under 1 atm H_2 (by $^{31}P\{^1H\}$ SSNMR spectroscopy) = 15 and 90 min, respectively.

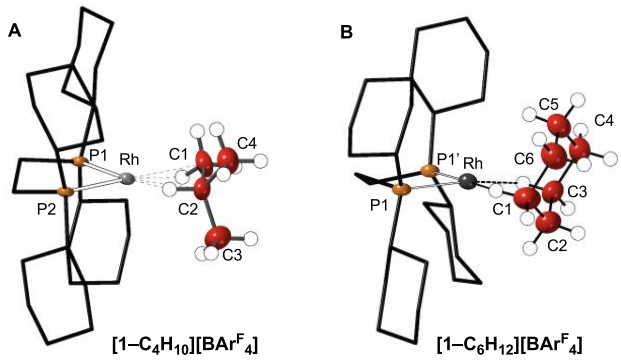

Figure 2. Solid-state structures of $[\mathbf{1}\text{-}C_4H_{10}][BAr^F{}_4]$ and $[\mathbf{1}\text{-}C_6H_{12}][BAr^F{}_4]$. Displacement ellipsoids shown at the 30% probability level. $[BAr^F{}_4]^-$ anions and most hydrogen atoms omitted for clarity. Only one disordered component shown. (A) $[\mathbf{1}\text{-}C_4H_{10}][BAr^F{}_4]$ (one of the independent cations): Rh1–P1, 2.1830(14); Rh1–P2, 2.1914(14); Rh1–C1, 2.362(14); Rh1–C2, 2.442(7); C1–C2, 1.551(13); C2–C3, 1.528(13); C2–C4, 1.516(13). (B) $[\mathbf{1}\text{-}C_6H_{12}]$-$[BAr^F{}_4]$: Rh1–P1, 2.191(2); Rh1–C1, 2.62(2); Rh1–C3, 2.53(2); C1–C2, 1.529(15); C2–C3, 1.531(15).

$[\mathbf{1}\text{-NBA}][BAr^F{}_4]$ that also shows a 1,2-η^2:η^2-coordination motif,[50] albeit through two methylene groups [2.389(3), 2.400(3) Å].[41] This description is also fully supported by electronic structure analyses (see Supporting Materials). The C–C distances in the alkane show single bonds [1.516(13)–1.551(13) Å]. The Rh–P distances in $[\mathbf{1}\text{-}C_4H_{10}][BAr^F{}_4]$ are shorter by ~0.04 Å than in $[\mathbf{1}\text{-}C_4H_8][BAr^F{}_4]$, reflecting the weaker trans influence of the alkane ligands. A chemically identical disordered component is related by a small rotation of the alkane (ca. 25°) around C2 (Figure S94). Hydrogen atoms were placed in calculated positions in the final refinement. Addition of H_2 is also signaled by a change in geometry around

DOI: 10.1021/jacs.9b05577
J. Am. Chem. Soc. 2019, 141, 11700–11712

the tertiary C-atom (C2) from sp^2 in $[\mathbf{1}\text{-}C_4H_8][BAr^F{}_4]$ to sp^3 in $[\mathbf{1}\text{-}C_4H_{10}][BAr^F{}_4]$: sum of angles around C2 = 360.0° and 335.1°, respectively. The $^{13}C\{^1H\}$ SSNMR spectrum shows a featureless alkene region (δ 110−50), while in the $^{31}P\{^1H\}$ SSNMR spectrum a major new broad signal is shifted 12 ppm to lower field compared to the starting alkene complex (δ 106.8). Notably, under these conditions a small amount of starting material and alkane-loss decomposition product in which the $[BAr^F{}_4]^-$ anion is coordinated with the metal center, $[\mathbf{1}\text{-}BAr^F{}_4]$,[41] are also observed (~10% total). Longer times for H_2 addition (90 min, 298 K) resulted in complete loss of crystallinity to give $[\mathbf{1}\text{-}BAr^F{}_4]$,[51] Scheme 3B, as measured by $^{31}P\{^1H\}$ SSNMR spectroscopy.

For $[\mathbf{1}\text{-}C_6H_{12}][BAr^F{}_4]$ the cyclohexane ligand is disordered over two positions (Figure 2 and Scheme 4A), related by a crystallographically imposed C_2 axis that, when coupled with the reduction in data quality inherent in SC-SC transformations (R = 10.3%), meant that the C−C distances in the alkane were necessarily restrained. Nevertheless, the coordination geometry is fully consistent with a σ-alkane ligand interacting via two C−H···Rh interactions in a 1,3-motif.[52] The Rh···C distances [2.62(2), 2.53(2) Å] are longer than in $[\mathbf{1}\text{-}C_4H_{10}][BAr^F{}_4]$, but similar to those in $[\mathbf{1}\text{-pentane}][BAr^F{}_4]$ [2.514(4), 2.522(5) Å] that also shows a 1,3-coordination mode for the alkane.[53] The $^{31}P\{^1H\}$ and $^{13}C\{^1H\}$ NMR spectra are consistent with this formulation, and are similar to $[\mathbf{1}\text{-}C_4H_{10}][BAr^F{}_4]$. Notably C═C environments that are observed in the $^{13}C\{^1H\}$ SSNMR spectrum of $[\mathbf{1}\text{-}C_6H_8][BAr^F{}_4]$ (96−81 ppm) disappear on addition of H_2 (Figures S22 and S25). Despite the longer Rh···C distances, $[\mathbf{1}\text{-}C_6H_{12}][BAr^F{}_4]$ is significantly less sensitive to displacement by H_2 than $[\mathbf{1}\text{-}C_4H_{10}][BAr^F{}_4]$, and after 90 min under H_2 only 10% decomposition is observed by $^{31}P\{^1H\}$ SSNMR (Scheme 3B and Figure S34).[51] This may reflect the weak, multiple, stabilizing dispersive interactions between the surface of cyclohexane and the proximal $[BAr^F{}_4]^-$ in the anion-microenvironment as we have previously commented on for other alkane-complexes.[42]

For both $[\mathbf{1}\text{-}C_4H_{10}][BAr^F{}_4]$ and $[\mathbf{1}\text{-}C_6H_{12}][BAr^F{}_4]$ addition of MeCN to the crystalline solids results in liberation of the free alkane as determined by ^1H NMR spectroscopy of the vacuum transferred volatiles. $[\mathbf{1}\text{-}C_4H_{10}][BAr^F{}_4]$ or $[\mathbf{1}\text{-}C_6H_{12}]$-$[BAr^F{}_4]$ are also not stable in CD_2Cl_2 solution, and zwitterionic $[\mathbf{1}\text{-}BAr^F{}_4]$, $[\mathbf{1}\text{-}(CH_2Cl_2)_n][BAr^F{}_4]$[54] and free alkane are observed by NMR spectroscopy upon dissolving in cold (183 K) CD_2Cl_2. Upon warming, these solutions decompose to give a mixture of products, as identified by electrospray ionization mass spectroscopy (ESI-MS), some of which come from C−Cl activation of the solvent.[55]

The alkane ligands in both the σ-complexes undergo motion in the solid-state, as we have noted previously for the norbornane ligand in $[\mathbf{1}\text{-NBA}][BAr^F{}_4]$ and related systems.[42,53,56] In the $^1H/^{13}C$ FSLG HETCOR SSNMR[59] spectrum of $[\mathbf{1}\text{-}C_6H_{12}][BAr^F{}_4]$ at 158 K a distinct correlation is observed between $\delta(^{13}C)$ 19.7 and two signals in the ^1H projection at δ −1.6/1.2, consistent with diastereotopic methylene groups in cyclohexane (i.e., axial and equatorial, Figures S29−S32). At 198 K these signals disappear, suggesting the onset of a fluxional process. A 158 K ^{13}C-NQS experiment, which probes the motion of (CH_n) groups in a frequency range similar to, or greater than, the $^1H-^{13}C$ dipolar coupling,[57] shows two signals at δ 21.4 and 19.7 that are assigned to the cyclohexane ligand. At 198 K only one signal is observed at δ 21.4 (Figures S27 and S28). These observations, combined with the disorder in the single-crystal X-ray structure, lead us to propose a combination of two low energy fluxional processes is occurring: a 1,3,5-"ring walk", which operates at 158 K, retains the fidelity of the diastereotopic methylene groups and does not exchange 1,3,5 and 2,4,6 positions; and a higher energy chair−chair "ring flip" that makes all the carbon positions equivalent (Scheme 4B). This latter fluxional process mirrors the observed disorder in the solid-state structure. Low energy fluxional processes in the solid-state have been reported for other σ-alkane, or related, complexes.[42,53,56] While these two processes make all the carbon environments equivalent on the NMR time scale, they do not exchange all the axial and equatorial C−H groups in the ring, and this model for the fluxional process leads to six C−H bonds that contact the metal center (highlighted in red, Scheme 5) and another set of six C−H bonds of the cyclohexane ligand that are always remote from the metal (blue). SSNMR calculations (periodic-DFT, GIPAW method) on the nearest-neighbor ion-pair derived from the optimized structure of $[\mathbf{1}\text{-}C_6H_{12}][BAr^F{}_4]$ reveal significant high field shifts for the C4−H_{ax} and C6−H_{ax} hydrogens that interact directly with the metal center,[20,21,41,56] with smaller high field shifts computed for the remote C1−H_{ax} and C3−H_{ax} positions. The latter are likely due to ring current effects from the nearby[58] anion aryl groups (Figure S33).[41] The computed average chemical shift for the H_{ax} and H_{eq} hydrogens at the C2, C4 and C6 positions is −4.3 and +0.8 ppm, respectively, in reasonable agreement with the values observed at 158 K.

For the isobutane ligand in $[\mathbf{1}\text{-}C_4H_{10}][BAr^F{}_4]$ two environments are observed in the 203 K ^{13}C-NQS spectrum in the

Scheme 4. (A) Crystallographically Imposed Cyclohexane Disorder in $[\mathbf{1}\text{-}C_6H_{12}][BAr^F{}_4]$; (B) Proposed Fluxional Process in the Solid-State

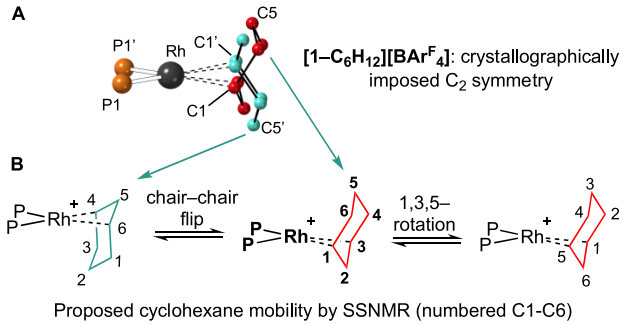

Scheme 5. Computed Chemical Shifts for $[\mathbf{1}\text{-}C_6H_{12}][BAr^F{}_4]$ and $[\mathbf{1}\text{-}C_4H_{10}][BAr^F{}_4]$

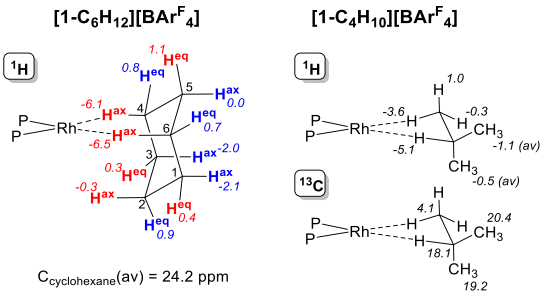

DOI: 10.1021/jacs.9b05577
J. Am. Chem. Soc. 2019, 141, 11700−11712

aliphatic region, at δ ~21 and ~15. At 158 K these signals disappear, suggesting an arrested low energy motion for the isobutane ligand in the solid-state. A $^{1}H/^{13}C$ FSLG HETCOR SSNMR experiment at 158 K shows a correlation between the signal at $\delta \sim 21$ (^{13}C) and δ −3.4 (^{1}H projection), similar to [**1-C$_6$H$_{12}$**][**BAr$^F_4$**], signaling a Rh···H−C interaction (Figures S11−S13). However, these experimental data do not map directly onto computed chemical shift averages for [**1-C$_4$H$_{10}$**][**BAr$^F_4$**] (Scheme 5). Given our recent success in calibrating computational and experimentally determined chemical shifts in σ-alkane complexes in the solid-state,[53,56] this discrepancy may point to a fluxional/equilibrium process that is occurring at low temperature that remains to be determined.

Short-lived, cyclic and branched σ-alkane complexes have been characterized in solution at low temperature (173 K or lower) by in situ NMR spectroscopy, e.g., (η^5-C$_5$H$_5$)Re(CO)$_2$(cyclohexane)[60] and (η^5-C$_5$H$_5$)Mn(CO)$_2$(isopentane),[61] or TRIR experiments, (η^5-C$_5$H$_5$)Rh(CO)(cycloalkane).[62] In such species the alkanes bind with the metal centers through M···H−C interactions in an ensemble of interconverting isomers; and similar to that suggested to occur for cyclohexane here, these interconvert by chain or ring walking, or axial/equatorial isomerization.

H/D Exchange in σ-Alkane Complexes. The isolation of [**1-C$_4$H$_{10}$**][**BAr$^F_4$**] and [**1-C$_6$H$_{12}$**][**BAr$^F_4$**] in the solid-state in synthetically meaningful amounts (up to 0.15 g) offers an opportunity to study C−H activation processes in σ-alkane complexes in the absence of competing pre-equilibria. Catalytic H/D exchange in alkanes using D_2 probes such processes by reversibly intercepting the corresponding metal−alkyl hydride intermediate that arises from C−H bond cleavage (Scheme 1B).[30] We have recently shown that [**1-NBA**][**BAr$^F_4$**] undergoes a remarkably selective *exo*-H/D exchange at the bound alkane on addition of D_2 in a solid/gas SC-SC reaction.[56] Addition of D_2 (298 K, 1 bar) to either [**1-C$_4$H$_{10}$**][**BAr$^F_4$**] or [**1-C$_6$H$_{12}$**][**BAr$^F_4$**] results in relatively rapid H/D exchange at all the C−H bonds of the bound alkane. This is best shown for crystalline [**1-C$_6$H$_{12}$**][**BAr$^F_4$**], where 3 successive additions of D_2 results in perdeuteration of the cyclohexane (optimized, 90 min total, 10% decomposition). This is conveniently measured by liberating the alkane on addition of MeCN to the crystalline solid (Scheme 6). Gas chromatography−mass spectrometry (GC−MS) analysis shows the formation of only one isotopologue, C_6D_{12} (m/z = 96.17), confirmed by the $^{13}C\{^{1}H\}$ NMR spectrum, which shows a quintet [δ 25.3; J(CD) = 19 Hz], and the ^{2}H NMR spectrum that shows a single environment for cyclohexane at δ 1.37. Shorter exposure times (3 × 5 min) resulted in a mixture of isotopologues for which D-incorporation increases monotonically, as measured by GC−MS (Figure S48). Interestingly, despite the shorter reaction times, the isotopologue distribution is dominated by 6-fold H/D exchange (i.e., $C_6H_6D_6$) and above. As the perdeuteration observed indicates all 12 C−H bonds are involved in H/D exchange an additional fluxional process that exchanges the faces of the cyclohexane under conditions of exogenous D_2 is necessary that, in combination with the 1,3,5-ring walk/chair−chair flip already described (Scheme 4), allows the metal center to access to all the methylene C−H positions. The distribution of isotopologues at short exposure times suggests this face exchange process is likely higher in energy than the other two process (1,3,5-rotation and chair−chair flip). These processes have been defined computationally, see later.

Scheme 6. H/D Exchange in the σ-Alkane Complexes, and Associated $^{13}C\{^{1}H\}$ NMR (and Simulated) Spectra of the Liberated Alkane[a]

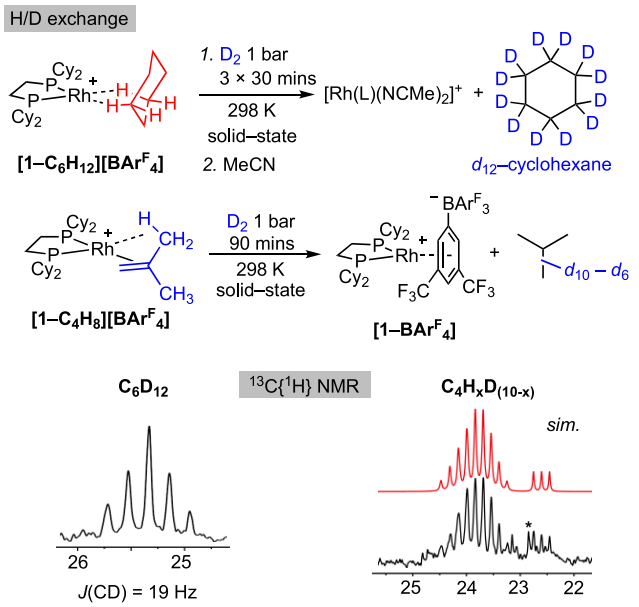

[a]Asterisk indicates pentane impurity.

For [**1-C$_4$H$_{10}$**][**BAr$^F_4$**] the limited stability of the isobutane σ-alkane complex under H_2 (D_2) meant that H/D exchange experiments started from the isobutene complex for experimental expediency. This formed a mixture of isobutane isotopologues, $C_4H_xD_{(10-x)}$ (x = 0−4, Figure S41), after 90 min, as measured by GC−MS of the volatiles after vacuum transfer into CD_2Cl_2. This distribution of isotopologues also increases monotonically. Beyond this time, complete decomposition by loss of alkane occurs to form [**1-BAr$^F_4$**]. The $^{13}C\{^{1}H\}$ NMR spectrum of volatiles liberated on addition of MeCN shows that H/D incorporation at both methine (C−H) and methyl (CH_3) groups under the timescale of the experiment, the former signaled by the observation of an apparent 1:1:1 triplet [δ 22.5; J(CD) = 20 Hz, Scheme 6]. Initial deuteration of isobutene places D in this position.[63] The methyl groups present a more complicated set of overlapping resonances that have been simulated with $CD_3/CD_2H/CDH_2$ in a 62:30:8 ratio. Two environments in a relative 1:9 ratio [δ 1.86, 0.85] are observed in the ^{2}H NMR spectrum, and are assigned to the *d*-methine and *d*-methyl, respectively (Figure S39). Again, there must be a fluxional process in the solid-state that allows for all the C−H bonds of the methyl groups to undergo H/D exchange; however, decomposition of the alkane complex under D_2 (H_2) atmosphere makes studying this less straightforward than for its cyclohexane analog. Nevertheless, the rotational disorder observed in the solid-state structure of [**1-C$_4$H$_{10}$**][**BAr$^F_4$**], coupled with the mobility suggested by NQS experiments and deuteration levels approaching C_4D_{10}, indicates that all methyl groups can contact the Rh-center.

For both cyclohexane and isobutane σ-alkane complexes stepwise H/D exchange with D_2 could occur either by oxidative addition of D_2 followed by σ-CAM[64] with a Rh···H−C bond, or via oxidative cleavage of an alkane C−H bond to form Rh−H species that are intercepted by D_2. The

DOI: 10.1021/jacs.9b05577
J. Am. Chem. Soc. 2019, 141, 11700−11712

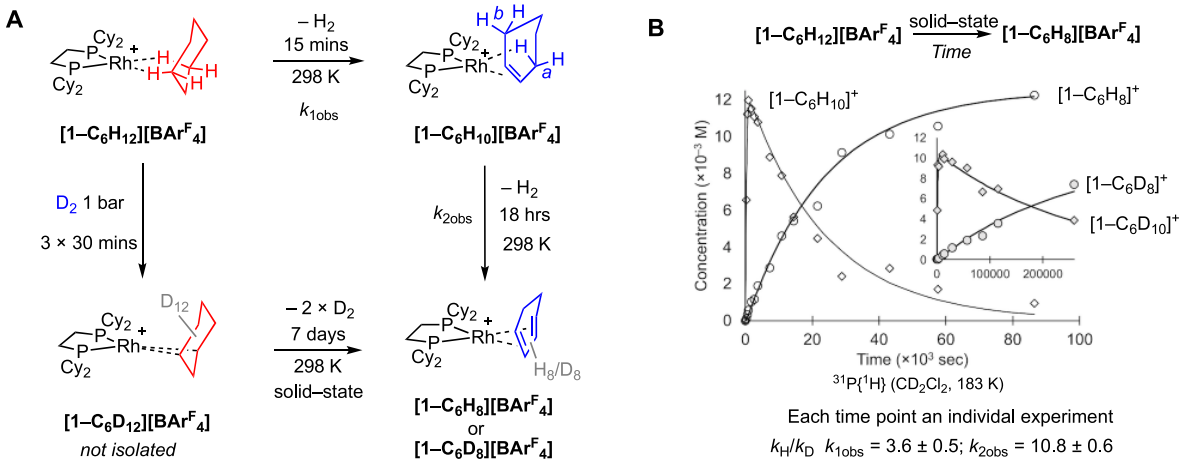

Figure 3. (A) Dehydrogenation of crystalline [**1**-C_6H_{12}][BAr^F_4] or in situ formed [**1**-C_6D_{12}][BAr^F_4] under Ar flow or vacuum (10^{-2} mbar). (B) Temporal plot of the solid-state dehydrogenation under vacuum, as measured by quantitative $^{31}P\{^1H\}$ NMR spectroscopy of dissolved sample (CD_2Cl_2, 183 K). Signals due to [**1**-$(CH_2Cl_2)_n$][BAr^F_4] are taken as a proxy for [**1**-C_6H_{12}][BAr^F_4] (not shown). Each time point is an individual experiment, calibrated to an internal standard of PPh_3 of known concentration in a flame-sealed capillary (d_6-acetone). Solid lines are simulated plots (COPASI[65]) for two consecutive first-order processes. Inset shows dehydrogenation of [**1**-C_6D_{12}][BAr^F_4].

alternative pairwise exchange would involve dehydrogenation to form an alkene that is then deuterated, as we and others have commented upon previously.[21,56] While the monotonic increase in partially deuterated isotopologues for both alkanes suggests stepwise exchange, as we show next alkane dehydrogenation is a remarkably facile process, and thus we cannot rule out either mechanism—or if both operate contemporaneously. Computational studies are underway to probe the precise mechanism of H/D exchange and will be reported in a future contribution.

Acceptorless Dehydrogenation of σ-Alkane Complexes. In the absence of H_2 or D_2, acceptorless dehydrogenation of the bound σ-alkane ligand occurs in the solid-state to reform the corresponding alkene complex. Although for both free isobutane and cyclohexane this is an endothermic process—and this remains the case when these are bound to a metal center (see Computational Section)—removal of the generated H_2 results in a remarkably fast (minutes to hours) dehydrogenation in the solid-state to reform the alkene complexes (Figure 3). This process is so facile that isolated [**1**-C_4H_{10}][BAr^F_4] and [**1**-C_6H_{12}][BAr^F_4], and their deuterated analogues, show measurable dehydrogenation under an Ar atmosphere after only 5 min at 298 K. Isolation of pure [**1**-C_4H_{10}][BAr^F_4], especially, is finely balanced: under an H_2 (or D_2) atmosphere complete alkane loss occurs over 90 min to form [**1**-BAr^F_4] while under Ar, or mild vacuum (10^{-2} mbar), dehydrogenation occurs on a comparable time scale. [**1**-C_6H_{12}][BAr^F_4] is more robust to alkane loss, meaning the dehydrogenation process is more reliably followed.

The dehydrogenation of [**1**-C_6H_{12}][BAr^F_4] can be monitored by solid-state and solution NMR spectroscopies by running multiple solid-state experiments in which the time of reaction is varied before dissolving in CD_2Cl_2 at 183 K by vacuum transfer of solvent onto the sample. For consistency, finely ground microcrystalline powder was used (10 mg), a dynamic vacuum was applied (10^{-2} mbar) to remove H_2 and low temperature (183 K, CD_2Cl_2, internal standard) quantitative $^{31}P\{^1H\}$ NMR spectroscopy of the dissolved samples was deployed to track progress. Under these low temperature measurement conditions the alkane complexes form the solvent adducts, [**1**-$(CH_2Cl_2)_n$][BAr^F_4], alongside [**1**-BAr^F_4], both of which act as a proxy for the σ-alkane complexes.[47] For [**1**-C_6H_{12}][BAr^F_4] these experiments show complete dehydrogenation to the diene [**1**-C_6H_8][BAr^F_4] in 16 h, which was fully characterized by solution NMR spectroscopy.[46] The dehydrogenation can also be tracked using in situ $^{31}P\{^1H\}$ and $^{13}C\{^1H\}$ SSNMR spectroscopy (Figures S67 and S68), but as long-range order is lost in the process, likely due to crystal cracking,[66] attempts to follow this by SC-SC X-ray diffraction experiments were not successful. The material does retain microcrystallinity, however,[67,68] as demonstrated by a powder X-ray diffraction experiment on the dehydrogenated sample.

The resulting temporal profile shows that after 15 min the principal component (~95%) is a new complex that can be fully characterized using low temperature solution NMR spectroscopy (183 K) to be the result of a single dehydrogenation, i.e., the cyclohexene complex [**1**-C_6H_{10}][BAr^F_4]. Addition of $CO_{(g)}$ in a solid/gas reaction after 15 min displaces the cyclohexene allowing for its full characterization by NMR spectroscopy and GC−MS (Figures S79−S82). By analogy with other mono-alkene complexes, we propose the cyclohexene in [**1**-C_6H_{10}][BAr^F_4] adopts an $\eta^2_\pi:\eta^2_{C-H}$ binding mode in which the π-interaction is supported by an agostic interaction from an adjacent methylene group. This structure is also located computationally (see Computational Section). Notable data include two mutually coupled environments in the $^{31}P\{^1H\}$ spectrum [δ 98.0, J(RhP) = 207 Hz; δ 91.5, J(RhP) = 159 Hz], while in the ^1H NMR spectrum a single alkene environment is observed (2H, δ 5.23, confirmed by heteronuclear single quantum coherence) and a resonance in the high field region of the ^1H NMR spectrum characteristic of a Rh···H−C agostic interaction (2H, δ −1.01). We propose a low energy libration of the alkene to account for this C_s symmetry observed in solution that exchanges C_a and C_b (Figure 3 and S69), as has been proposed for the closely associated [**1**-(***cis*-2-butene**)][BAr^F_4] analogue where the calculated barrier to libration is 3 kcal mol^{-1}.[47] Warming solutions resulted in decomposition to [**1**-C_6H_8][BAr^F_4], the benzene complex [**1**-C_6H_6][BAr^F_4] (independently synthesized) and [**1**-BAr^F_4].

DOI: 10.1021/jacs.9b05577
J. Am. Chem. Soc. 2019, 141, 11700−11712

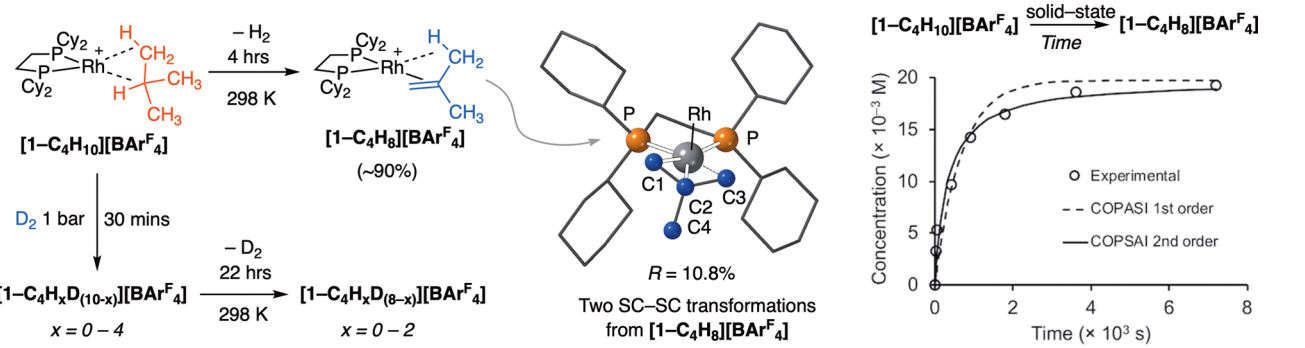

Figure 4. Dehydrogenation of crystalline [**1**-C_4H_{10}][BAr^F_4] under Ar-flow or vacuum (10^{-2} mbar). Solid-state structure of [**1**-C_4H_8][BAr^F_4] formed in a SC-SC transformation (ball and stick). Temporal plot of the solid-state dehydrogenation under vacuum. Lines are simulated plots (COPASI[65]) for first-order process (dashed), second-order process (solid).

The corresponding perdeuterated analogue, [**1**-C_6D_{12}]-[BAr^F_4], also undergoes dedeuteration in the solid-state, but much more slowly, taking 7 days to afford [**1**-C_6D_8][BAr^F_4], as shown by ESI-MS, ^{1}H, ^{2}H and ^{31}P{^{1}H} solution NMR spectra (Figure 3). In the ^{13}C{^{1}H} NMR spectrum three environments are observed at δ 94.7 [1:1:1 triplet, J(CD) = 26 Hz], δ 82.3 [1:1:1 triplet, J(CD) = 23 Hz], δ 21.3 [1:2:3:2:1 quintet, J(CD) ~ 20 Hz] assigned to the two pairs of =CD and CD_2 groups, respectively (Figure S87). That the bound, deuterated diene is also seen after addition of D_2 to [**1**-C_6H_{12}][BAr^F_4], shows that the σ-alkane interactions must persist on H/D exchange prior to undergoing dehydrogenation.

By using a solution-based kinetics model, the temporal evolution of the dehydrogenation of [**1**-C_6H_{12}][BAr^F_4] to give first [**1**-C_6H_{10}][BAr^F_4] and then [**1**-C_6H_8][BAr^F_4] in the solid-state as measured by the individual trapping experiments can be simulated, using COPASI,[65] by two consecutive first-order processes with k_{1obs} = 3.1(2) × 10^{-3} s^{-1} and k_{2obs} = 4.2(2) × 10^{-5} s^{-1}.[69] These correspond to $\Delta G^{\ddagger}$ (298 K) of 21 and 24 kcal mol^{-1}, respectively, for these two overall C–H activation processes. Dedeuteration from the (not isolated) per-deuterated σ-alkane complex [**1**-C_6D_{12}][BAr^F_4] can also be modeled by two (slower) first-order processes, and this allows for a significant kinetic isotope effect (KIE) to be determined for these two overall dehydrogenation processes: KIE (k_{1obs}) = 3.6(5) and KIE (k_{2obs}) = 10.8(6). The first dehydrogenation (k_{1obs}) has a KIE similar to other cyclohexane mono-dehydrogenations, e.g., photodehydrogenation using *trans*-$Rh(PMe_3)_2(CO)Cl$ (k_H/k_D = 5.3)[9] and photo- or transfer-dehydrogenation using $Ir(PR_3)_2(H)_2(O_2CCF_3)$ (k_H/k_D = 4.4–7.7).[6] The second dehydrogenation of the cyclohexene shows a larger kinetic isotope effect. While this may indicate a small tunnelling contribution, similarly large KIEs have been reported for photochemically promoted C–H activations at $Cp^*Rh(CO)_2$,[26,33] or C–H activation of methane in $Cp^*_2ScCH_2CMe_3$.[70] The details of these dehydrogenation mechanisms are discussed in the Computational Study.

A remarkably straightforward dehydrogenation process also occurs from the isobutane complex [**1**-C_4H_{10}][BAr^F_4], so that after 4 h complete H_2 loss has occurred in the solid-state to give [**1**-C_4H_8][BAr^F_4] (Figure 4). This occurs under a mild dynamic vacuum (10^{-2} mbar), as for the cyclohexane analogue, and can be followed using solution trapping or solid-state NMR spectroscopy. This provides data suitable for a quantitative analysis, by measuring the concentrations of [**1**-C_4H_8][BAr^F_4] for different samples where the time of dehydrogenation is varied. This also occurs in an Ar-flow, resulting in a similar temporal profile. Unlike for [**1**-C_6H_{12}][BAr^F_4] this SC-SC process retains enough long-range order to confirm the structure of the isobutene complex by single-crystal X-ray diffraction, and this is essentially identical to that prepared independently (see earlier), albeit with a poorer structural solution (R = 10.8%, twinned crystals), Figure 4. Surprisingly to us, this dehydrogenation process is best modeled as following overall second-order classical solution-based kinetics (i.e., second order in [**1**-C_4H_{10}]-[BAr^F_4]), $k_{(obs)}$ = 1.6(2) × 10^{-4} M^{-1} s^{-1}, and Figure 4 shows a COPASI modeled fit to both first- and second-order processes. The same process occurs from partially deuterated [**1**-$C_4H_xD_{(10-x)}$][BAr^F_4] (***x*** **= 0–4**), formed from 30 min addition of D_2 to [**1**-C_4H_{10}][BAr^F_4], to give [**1**-$C_4H_xD_{(8-x)}$]-[BAr^F_4] (x = 0–0–2). This partial deuteration meant that experiments to determine a KIE were not attempted.

The dehydrogenation of these σ-alkane complexes in the solid-state has also been modeled using modified Johnson–Mehl–Avrami–Kologoromov (JMAK) kinetics,[71−73] which express the progress (i.e., conversion) of solid-state reactions in terms of a nucleation and growth model (eq 1, Figure 5):

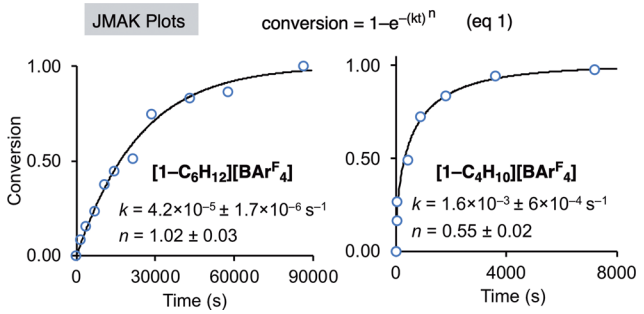

Figure 5. Modified JMAK plot[71] of conversion versus time for the second dehydrogenation of [**1**-C_6H_{12}][BAr^F_4] and dehydrogenation of [**1**-C_4H_{10}][BAr^F_4]. k = growth rate constant, n = Avrami exponent. Details as in Figure 3.

where k is the growth rate constant and n is the Avrami exponent. Exponents close to n = 4, 3 and 2 are suggestive of 3-D, 2-D and 1-D growth, respectively, while n = 1 is indicative of a noncooperative transformation that occurs throughout the crystal, and can be related to a classical first-order process in homogeneous systems.[74] Pertinently, JMAK analysis has been used to describe SC-SC photoreactions in the solid-state,[75−77] while Finke has discussed the relationship between solid-phase reaction progress and classical chemical kinetics, especially the

DOI: 10.1021/jacs.9b05577
J. Am. Chem. Soc. 2019, 141, 11700–11712

connections between k/n and rate constants/order in reaction.[73] Given the small number of data points for the first rapid dehydrogenation of $[\mathbf{1}\text{-}C_6H_{12}][BAr^F{}_4]$, only the second dehydrogenation was modeled using JMAK reaction kinetics, and this yielded $n = 1.02(3)$ with an associated growth rate constant, k, of $4.2(2) \times 10^{-5}$ s^{-1} which is also an excellent fit with that determined using classical chemical kinetics (Figure 5, k_{2obs}), i.e., first order. We interpret this as each lattice point in the crystalline material acting independently for this second dehydrogenation step. For isobutane dehydrogenation in $[\mathbf{1}\text{-}C_4H_{10}][BAr^F{}_4]$, different solid-state kinetics are determined: $n = 0.55(3)$ with an associated growth rate constant, k, of $1.6(6) \times 10^{-3}$ s^{-1}, which is not directly relatable to a classical rate constant given that $n \neq 1$.[74] It has been suggested that such noninteger Avrami constants point to the kinetics being diffusion controlled.[72] It is interesting to note that this process can also be modeled using second-order classical kinetics (vide supra), which may point to a cooperative process for H_2 loss in the single crystal. While we currently are reluctant to overinterpret these observations, they could be related to a reaction front (i.e., H_2 loss) that moves through the crystal from outside to in, as we have previously demonstrated empirically by CO addition to an analogue of $[\mathbf{1}\text{-}C_6H_8][BAr^F{}_4]$.[78] Differences in the second[69] dehydrogenation process between $[\mathbf{1}\text{-}C_6H_{12}][BAr^F{}_4]$ ($n = 1$) and $[\mathbf{1}\text{-}C_4H_{10}][BAr^F{}_4]$ ($n \sim 0.5$) may be related to the loss of long-range order in the former on dehydrogenation, likely via crystal degradation that exposes new crystal surfaces,[66] that may result in H_2 loss processes being less important to reaction progress.

Computational Studies: Thermodynamics and Mechanism of Dehydrogenation. The thermodynamics of H_2 loss from $[\mathbf{1}\text{-}C_6H_{12}][BAr^F{}_4]$, $[\mathbf{1}\text{-}C_6H_{10}][BAr^F{}_4]$ and $[\mathbf{1}\text{-}C_4H_{10}][BAr^F{}_4]$ were computed with periodic DFT calculations with the PBE-D3 functional. Extended solid-state structures were fully optimized in all cases based on experimental crystallographic data, with the exception of $[\mathbf{1}\text{-}C_6H_{10}][BAr^F{}_4]$ where an initial geometry was constructed from $[\mathbf{1}\text{-}C_6H_{12}][BAr^F{}_4]$ via removal of H_2 from each cyclohexane ligand while maintaining the space group symmetry.[79] Optimized geometries for $[\mathbf{1}\text{-}C_6H_{12}][BAr^F{}_4]$ and $[\mathbf{1}\text{-}C_4H_{10}][BAr^F{}_4]$ provided good agreement with the experimental structures and, moreover, showed lengthening of the C−H bonds in contact with Rh (to 1.14−1.16 Å) that is consistent with σ-complex formation. This was also confirmed by electronic structure analyses (see Supporting Information).[50] Including the solid-state environment in these calculations is essential. For example, optimizations on the isolated $[\mathbf{1}\text{-}C_6H_{12}]^+$ cation show cyclohexane to prefer a 1,2-binding mode in which a C−C bond lies parallel to the Rh coordination plane, while in the solid-state this structure is strongly disfavored (see Figure 9 and the discussion below). In $[\mathbf{1}\text{-}C_6H_{10}][BAr^F{}_4]$ the cyclohexene ligand binds to the Rh center in an $\eta^2{}_\pi{:}\eta^2{}_{C-H}$ mode consistent with the NMR data measured for this species.

Figure 6 shows the computed free energies for dehydrogenation expressed both in terms of ΔG, the free energy change for dehydrogenation of a complete unit cell, and ΔG^{Rh}, the average free energy loss per Rh center (i.e., $\Delta G/Z$). ΔG^{Rh} = +6.3 kcal/mol for $[\mathbf{1}\text{-}C_6H_{12}][BAr^F{}_4]$ and +6.7 kcal/mol for $[\mathbf{1}\text{-}C_6H_{10}][BAr^F{}_4]$. Thus, both dehydrogenation processes are endergonic, but still accessible thermodynamically upon removing H_2 from the system.

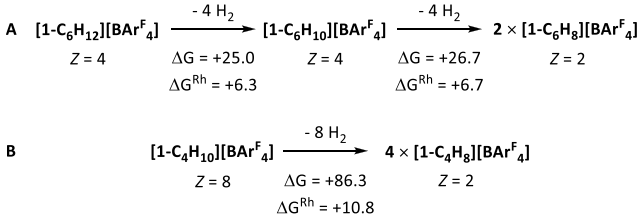

Figure 6. Computed thermodynamics of H_2 loss (kcal/mol) from (A) $[\mathbf{1}\text{-}C_6H_{12}][BAr^F{}_4]$ and (B) $[\mathbf{1}\text{-}C_4H_{10}][BAr^F{}_4]$ expressed as ΔG, the overall free energy change per unit cell, and ΔG^{Rh}, the free energy change per Rh center. See Supporting Information for a comparison of computed and observed metrics.

For the mechanisms of the sequential dehydrogenations of $[\mathbf{1}\text{-}C_6H_{12}][BAr^F{}_4]$ the experimental KIE data clearly signal significant C−H bond extension in the rate-determining steps for H_2 loss; however, they do not allow us to discriminate between C−H oxidative cleavage or β-H transfer as being rate limiting. Periodic DFT calculations were therefore employed to construct free energy profiles for these processes. These calculations used our previously published protocol,[56] i.e., for $[\mathbf{1}\text{-}C_6H_{12}][BAr^F{}_4]$ dehydrogenation at one of the Rh cations within the unit cell is considered while the remaining cell contents were free to relax within a unit cell that was constrained at its experimental dimensions.

Figure 7A shows the computed free energy profile for dehydrogenation in $[\mathbf{1}\text{-}C_6H_{12}][BAr^F{}_4]$, denoted **I** in the computational study. This commences with oxidative cleavage of the $C-H^1$ bond via **TS(I-II)** at +20.6 kcal/mol to give the hydrido alkyl intermediate **II** at +15.0 kcal/mol.[80] A facile rearrangement then brings the $C-H^2$ bond into contact with the Rh center (**III**, +11.0 kcal/mol) and permits β-H transfer via **TS(III-IV)** at +13.6 kcal/mol. This forms the Rh(III) dihydride intermediate **IV** at +8.3 kcal/mol in which the cyclohexene engages in an additional agostic interaction via the $C-H^5$ bond. H−H reductive coupling then provides η^2-H_2 complex **V** from which H_2 dissociates via **TS(V-VI$_a$)** at +16.7 kcal/mol to give the cyclohexene adduct **VI$_a$** which, once the H_2 molecule is removed from the lattice,[81] has a free energy of +2.8 kcal/mol.[82] The overall dehydrogenation barrier of 20.6 kcal/mol agrees well with the value derived from experiment (21 kcal/mol) and the rate limiting transition state features a $C\cdots H^1$ distance of 1.70 Å that is consistent with a significant k_H/k_D KIE.[80] The computed structure of **TS(I-II)** (Figure 7A, right) also highlights the proximity of the $[BAr^F{}_4]$ anion within the solid-state environment, and indeed this and other stationary points along the profile all exhibit a number of H···F contacts below the sum of the van der Waals radii (2.7 Å). A comparison of the solid-state profile in Figure 7A with that computed with the isolated cation (see Figures S97−S104) reveals several important differences. In the latter, facile rearrangement to more stable alternative 1,2-bis σ-cyclohexane complexes is computed from which C−H oxidative cleavage can proceed through a transition state at +9.7 kcal/mol. With this model the final H_2 loss becomes rate-limiting with $\Delta G^{\ddagger}{}_{span}$ = +19.6 kcal/mol. Thus, although the overall barrier is reasonable, a simple molecular model fails to account for the observed KIE and even predicts the wrong geometry for the alkane complex (see also the discussion of cyclohexane rearrangements in Figure 9).

Figure 7B shows the equivalent free energy profile for the dehydrogenation of cyclohexene in the full $[\mathbf{1}\text{-}C_6H_{10}][BAr^F{}_4]$

DOI: 10.1021/jacs.9b05577
J. Am. Chem. Soc. 2019, 141, 11700−11712

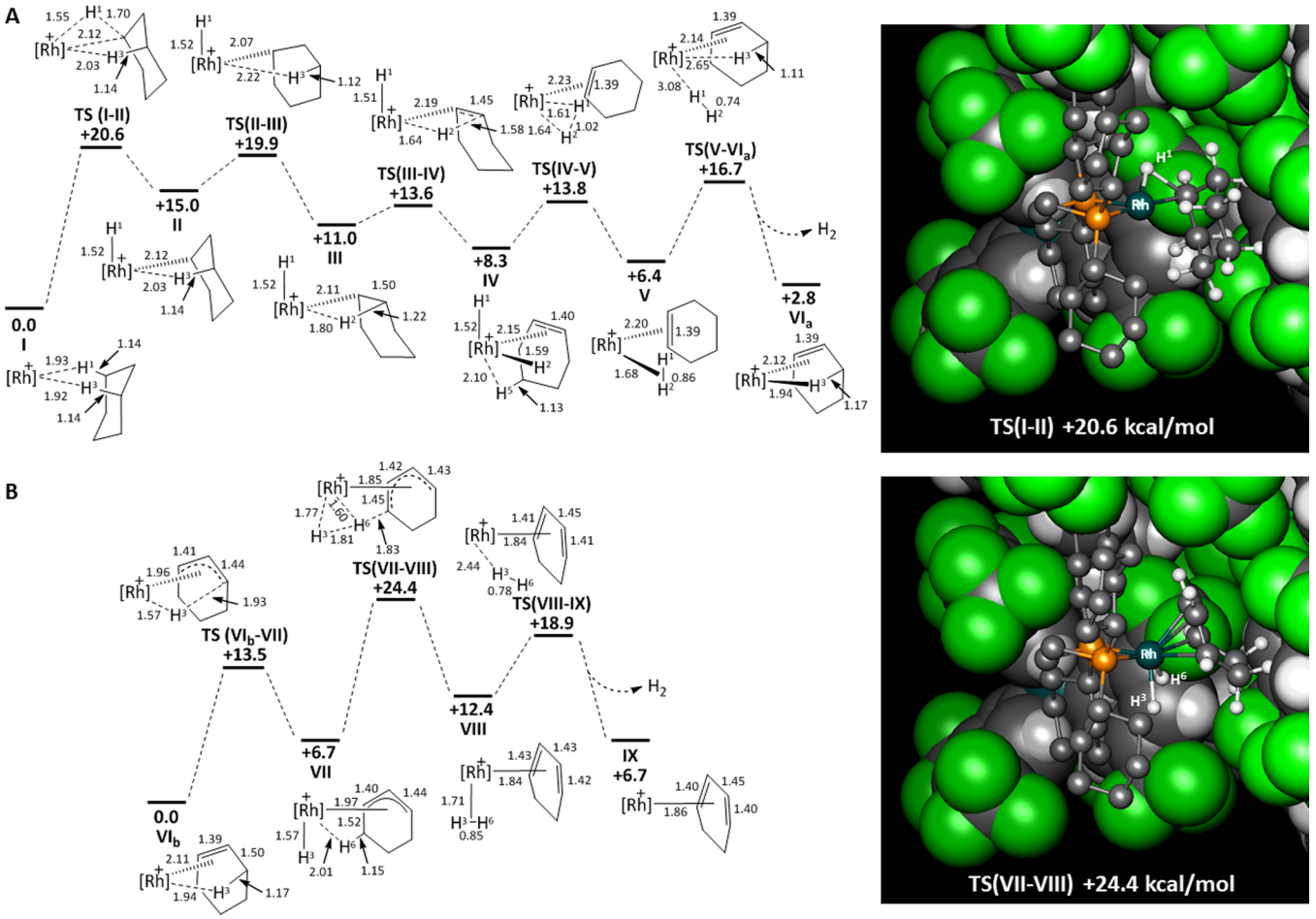

Figure 7. Free energy profiles (kcal/mol) for the dehydrogenation of (A) cyclohexane at one Rh center within the [**1**-C_6H_{12}][$BAr^F{}_4$] unit cell and (B) cyclohexene at one Rh center within the [**1**-C_6H_{10}][$BAr^F{}_4$] unit cell. Selected distances (Å) within the reacting Rh cations are shown, where $[Rh]^+ = [(Cy_2P(CH_2)_2PCy_2)Rh]^+$ and the remaining cell contents are omitted for clarity. Distances to delocalized π-ligands are to the centroid of the carbons involved. Also shown are the computed structures of the rate-limiting transition states for each profile, with the reacting Rh cation (ball and stick mode) set against the nearby unit cell contents (space-filling mode): Rh (teal); P (orange); C (charcoal); H (silver); F (green).

unit cell. Starting from this species (denoted **VI$_b$**), initial C−H^3 bond activation forms allyl hydride **VII** at +6.7 kcal/mol, which features an *exo*-orientation of the allyl ligand (i.e, with the central C−H oriented away from the Rh−H bond).[83] This allows the C−H^6 bond to engage in an agostic interaction *cis* the Rh-hydride and so permits H-transfer via a σ-CAM mechanism to form η^2-H_2 cyclohexadiene species **VIII** at +12.4 kcal/mol. H_2 dissociation and expulsion from the lattice forms **IX** at +6.7 kcal/mol. The overall barrier to dehydrogenation is 24.4 kcal/mol via **TS(VII−VIII)** and so provides excellent agreement with the activation barrier derived from experiment (24 kcal/mol). **TS(VII−VIII)** again exhibits significant C−H bond elongation (C···H^6 = 1.83 Å), but in this case this rate determining transition state is preceded by a pre-equilibrium involving reversible C−H oxidative cleavage. We therefore suggest that the observed large isotope effect of 10.8 ± 0.6 arises from a combination of an equilibrium isotope effect and a KIE. A similar scenario has been offered for the isotope effect measured in photochemically driven cyclohexane dehydrogenation using *trans*-$Rh(PMe_3)_2(CO)Cl$.[9]

Calculations also probed the fluxional processes involving the cyclohexane ligand in [**1**-C_6H_{12}][$BAr^F{}_4$]. The most accessible of these involves exchange of the three axial sites interacting with Rh via a 1,3,5-ring walk process and occurs with a very low barrier of 3.7 kcal/mol (see Figure 8A). This rotation also involves movement of the cyclohexane ring relative to the Rh coordination such that the intermediate 3,5-chair structure (coincidentally at 0.0 kcal/mol) has the cyclohexane moiety oriented as seen in the second disordered component defined crystallographically (although note that in this calculation only one of the four Rh centers is accessing this geometry). To higher energy is a ring flip process by which the axial and equatorial hydrogens on one face of the cyclohexane are exchanged. This proceeds through a twist-boat bis-σ-complex at +5.7 kcal/mol that is bound through the C−H^3 and C−H^6 bonds; this reflects a coupling of the half-chair transition state with a counterclockwise rotation of the cyclohexane moiety. From this intermediate a further half-chair transition state can be located that retrieves a chair conformation and establishes a Rh···H^4−C σ-interaction. This entails a clockwise rotation and again moves the cyclohexane above the Rh coordination plane[84] to the "disordered" structure.

Finally a mechanism for exchanging all 12 C−H positions was investigated, as required by the observation of per-deuterated C_6D_{12} experimentally. This requires a face-flip process whereby the set of six C−H bonds accessible via the 1,3,5-ring walk and ring flip processes are exchanged with the

DOI: 10.1021/jacs.9b05577
J. Am. Chem. Soc. 2019, 141, 11700−11712

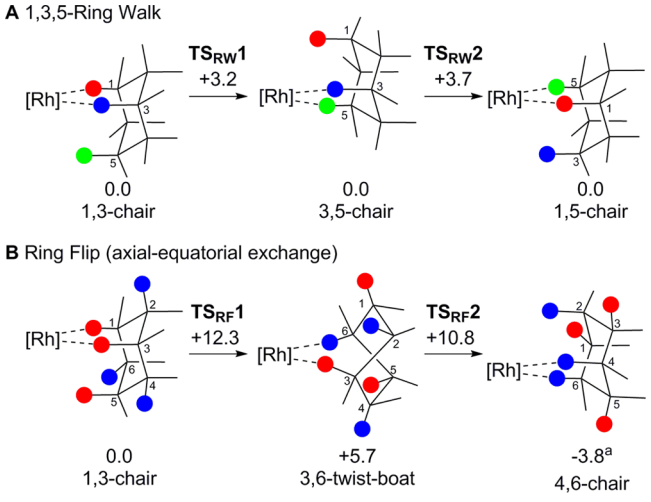

Figure 8. Computed pathways for cyclohexane rearrangements in [**1-C_6H_{12}**][BAr^F_4] via (A) 1,3,5-ring walk and (B) ring flip mechanisms, with free energies indicated in kcal/mol. [a]The SCF electronic energy of this 4,6-chair structure places it 2.1 kcal/mol above the 1,3-chair; however, a large stabilization due to thermodynamic corrections gives this anomalously low free energy.[84]

six C−H bonds that are initially remote from the metal center. In principle this could proceed via initial formation of a 1,2-bis σ-complex featuring Rh···H^{eq}−C^2 Rh···H^{ax}−C^1 interactions followed by rotation around the C^1−C^2 vector (see upper pathway, Figure 9). Such a process is readily accessible when

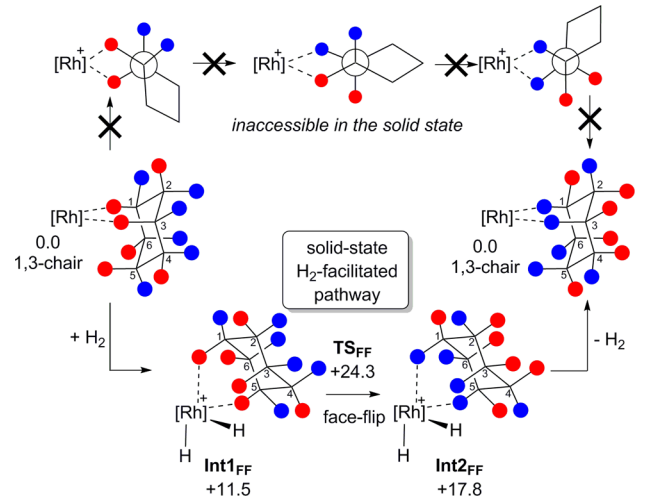

Figure 9. Pathways for the cyclohexane face-flip in [**1-C_6H_{12}**][BAr^F_4]. The upper pathway shows potential 1,2-bis σ-intermediates as Newman projections looking down the C^2−C^1 bond, but which proved inaccessible in the solid-state. The lower pathway shows the proposed H_2-facilitated pathway with free energies in kcal/mol. See text for details.

computed in the isolated cation; however, in the solid-state none of these structures is a minimum and attempts to compute the central bis equatorial σ-complex gave energies at least 30 kcal/mol above the 1,3-reactant. This reflects the proximity of the $[BAr^F_4]^-$ anion in the solid-state that does not permit the perpendicular orientation of the cyclohexane demanded by this pathway and again emphasizes the importance of taking the full solid-state environment into account when modeling these SMOM systems.

Instead we found that a face-flip process could be accessed upon addition and oxidative cleavage of H_2. The resultant Rh(III) dihydride intermediate allows more flexibility for cyclohexane movement including access to additional σ-interactions in the axial sites (see lower pathway, Figure 9). The face-flip transition state, TS_{FF}, again involves rotation about the C^1−C^2 vector, but now that the ligand can access space above the Rh coordination plane this proves to be accessible within the solid-state pocket and proceeds with an overall computed barrier of 24.6 kcal/mol. Thus, access to the remote ("blue") face of the cyclohexane ligand has a considerably higher barrier than rearrangements between the closer ("red") C−H bonds and this is consistent (assuming facile H/D exchange mechanisms) with the very rapid formation of $C_6H_6D_6$ upon exposure of [**1-C_6H_{12}**][BAr^F_4] to D_2, but the somewhat slower rate of formation of the higher $C_6H_xD_{(12-x)}$ isotopologues (x = 0−5).

CONCLUSIONS

We report here the industrially relevant, low temperature, acceptorless, dehydrogenation of the light alkanes isobutane and cyclohexane when bound as σ-complexes to a Rh(I) center. This demonstrates the advantages of solid-state organometallic chemistry (SMOM-chem) for the synthesis, characterization and subsequent reactivity of well-defined σ-complexes. Such species are traditionally short-lived when synthesized using in situ solution techniques at very low temperature, due to facile displacement of the weakly bound alkane by solvent or other exogenous ligand,[60,61] making onward exploration of structure and reactivity very challenging. It is, without doubt, the microenvironment provided by the $[BAr^F_4]^-$ anions in the solid-state that allows for this chemistry of M···H−C alkane interactions described here to be developed.

By biasing the pre-equilibrium completely to the side of alkane binding in the solid-state, a number of important observations can be made. Experimental and computational studies show that both alkane ligands can access low energy fluxional processes in the solid-state that allow all the C−H bonds to come into contact with the metal center. This, in turn, permits per-deuteration by H/D exchange using D_2, indicating that C−H oxidative cleavage of the bound alkane must also be a relatively low energy process. When followed by β-H-elimination alkane dehydrogenation occurs—an overall endothermic process that normally requires very high temperatures, or (at lower temperatures) a sacrificial acceptor. The SMOM approach thus promotes both (i) alkane complex formation and (ii) the easy removal of liberated H_2 by simple application of vacuum or Ar-flow: two consecutive processes that are necessary for the observed reactivity. With the cyclohexane σ-complex dehydrogenation occurs via a cyclohexene intermediate to give the corresponding cyclohexadiene product. Coupling these dehydrogenations with prior per-deuteration allows for k_H/k_D KIEs of 3.6(5) and 10.8(6), respectively, to be determined. Periodic DFT calculations identify rate-limiting C−H oxidative cleavage (for cyclohexane dehydrogenation) and β-H transfer (for cyclohexene dehydrogenation). The large KIE of the latter arises from the combination of significant C−H bond elongation in rate-limiting transition state with a pre-equilibrium that also involves C−H oxidative cleavage. The importance of solid-state computational studies, which capture the holistic microenvironment, compared with those on an isolated cation

DOI: 10.1021/jacs.9b05577
J. Am. Chem. Soc. 2019, 141, 11700−11712

(i.e., so-called "gas phase") is reflected by the excellent agreement between computation and experiment studies in probing the rate-limiting step, which is not captured in the absence of the solid-state environment.

While driving catalytic (acceptorless) dehydrogenation by removal of H_2,[13] working in the solid-phase,[85] or under continuous-flow gas phase conditions at high temperatures,[86] are not new concepts, that stoichiometric dehydrogenation occurs at such well-defined σ-alkane complexes in the solid-state at 25 °C suggests opportunities to develop this process catalytically at lower temperatures. Fine-tuning of the metal ligand coordination environment in the single-crystalline phase,[42] coupled with the possibilities offered by expediently removing H_2, offer potential solutions to move from stoichiometric to catalytic regimes in the single-crystalline state. Encouraging this approach, we have recently shown that SMOM-systems are highly effective solid/gas alkene-isomerization catalysts.[47] Overcoming the acknowledged problems of product (alkene) inhibition,[5] and understanding how gaseous reagents/products move in and out of the nonporous crystalline lattice are future challenges that we are currently focused on resolving.

■ ASSOCIATED CONTENT

Supporting Information

The Supporting Information is available free of charge on the ACS Publications website at DOI: 10.1021/jacs.9b05577.

Full details of experimental methods, characterization data, details of computational methods and experiments and single-crystal X-ray diffraction collection and refinement data (PDF)
Crystal X-ray diffraction data (CIF)
Computed Carteasian Coordinates (XYZ)
Movie S1 (MP4) C_6H_{12} face-flip
Movie S2 (MP4) C_6H_{12} chair-flip 1
Movie S3 (MP4) C_6H_{12} chair-flip 2
Movie S4 (MP4) C_6H_{12} ring walk

■ AUTHOR INFORMATION

Corresponding Authors

*andrew.weller@chem.ox.ac.uk
*S.A.Macgregor@hw.ac.uk

ORCID

Alasdair I. McKay: 0000-0002-6859-172X
Alexander J. Bukvic: 0000-0002-5717-2474
Bengt E. Tegner: 0000-0002-6880-9741
Arron L. Burnage: 0000-0001-7136-2402
Antonio J. Martínez-Martínez: 0000-0002-0684-1244
Stuart A. Macgregor: 0000-0003-3454-6776
Andrew S. Weller: 0000-0003-1646-8081

Author Contributions

§These authors contributed equally.

Notes

The authors declare no competing financial interest.

■ ACKNOWLEDGMENTS

We thank the EPSRC (EP/M024210, EP/K035908, EP/K035681), the Leverhulme Trust (RPG-2015-447) and SCG Chemicals Co., Ltd, Thailand for funding. This work used the ARCHER UK National Supercomputing Service (http://www.archer.ac.uk) and the Cirrus UK National Tier-2 HPC Service at EPCC (http://www.cirrus.ac.uk) funded by the University of Edinburgh and EPSRC (EP/P020267/1). We thank Dr. Graham Tizzard (UK National Crystallographic Service) for data collection on $[\mathbf{1\text{-}C_6H_8}][\mathbf{BAr^F{}_4}]$, and Dr. Hamish Yeung for valuable discussions on solid-state kinetics.

■ REFERENCES

(1) Goldberg, K. I.; Goldman, A. S. Large-Scale Selective Functionalization of Alkanes. *Acc. Chem. Res.* **2017**, *50*, 620−626.
(2) Sattler, J. J. H. B.; Ruiz-Martinez, J.; Santillan-Jimenez, E.; Weckhuysen, B. M. Catalytic Dehydrogenation of Light Alkanes on Metals and Metal Oxides. *Chem. Rev.* **2014**, *114*, 10613−10653.
(3) *NIST Chemistry Webbook*; Nist Standard Reference Database Number 69; Linstron, P. J., Mallard, W. G., Eds.; National Institute of Standards and Technol.ogy: Gaithersburg, MD, https://doi.org/10.18434/T4D303, (accessed November 23, 2018).
(4) Searles, K.; Chan, K. W.; Mendes Burak, J. A.; Zemlyanov, D.; Safonova, O.; Copéret, C. Highly Productive Propane Dehydrogenation Catalyst Using Silica-Supported Ga−Pt Nanoparticles Generated from Single-Sites. *J. Am. Chem. Soc.* **2018**, *140*, 11674−11679.
(5) Kumar, A.; Bhatti, T. M.; Goldman, A. S. Dehydrogenation of Alkanes and Aliphatic Groups by Pincer-Ligated Metal Complexes. *Chem. Rev.* **2017**, *117*, 12357−12384.
(6) Burk, M. J.; Crabtree, R. H. Selective Catalytic Dehydrogenation of Alkanes to Alkenes. *J. Am. Chem. Soc.* **1987**, *109*, 8025−8032.
(7) Zhou, X.; Malakar, S.; Zhou, T.; Murugesan, S.; Huang, C.; Emge, T. J.; Krogh-Jespersen, K.; Goldman, A. S. Catalytic Alkane Transfer Dehydrogenation by PSP-Pincer-Ligated Ruthenium. Deactivation of an Extremely Reactive Fragment by Formation of Allyl Hydride Complexes. *ACS Catal.* **2019**, *9*, 4072−4083.
(8) Solowey, D. P.; Mane, M. V.; Kurogi, T.; Carroll, P. J.; Manor, B. C.; Baik, M.-H.; Mindiola, D. J. A New and Selective Cycle for Dehydrogenation of Linear and Cyclic Alkanes under Mild Conditions Using a Base Metal. *Nat. Chem.* **2017**, *9*, 1126.
(9) Maguire, J. A.; Boese, W. T.; Goldman, A. S. Photochemical Dehydrogenation of Alkanes Catalyzed by Trans-Carbonylchlorobis-(Trimethylphosphine)Rhodium: Aspects of Selectivity and Mechanism. *J. Am. Chem. Soc.* **1989**, *111*, 7088−7093.
(10) Chowdhury, A. D.; Julis, J.; Grabow, K.; Hannebauer, B.; Bentrup, U.; Adam, M.; Franke, R.; Jackstell, R.; Beller, M. Photocatalytic Acceptorless Alkane Dehydrogenation: Scope, Mechanism, and Conquering Deactivation with Carbon Dioxide. *ChemSusChem* **2015**, *8*, 323−330.
(11) Rábay, B.; Braun, T.; Falkenhagen, J. P. Photolytic C−H Activation and Dehydrogenation of Alkanes at Cyclopentadienyl Iridium Complexes in a Perfluorinated Solvent. *Dalton Trans.* **2013**, *42*, 8058−8065.
(12) Xu, W.-W.; Rosini, G. P.; Krogh-Jespersen, K.; Goldman, A. S.; Gupta, M.; Jensen, C. M.; Kaska, W. C. Thermochemical Alkane Dehydrogenation Catalyzed in Solution without the Use of a Hydrogen Acceptor. *Chem. Commun.* **1997**, 2273−2274.
(13) Aoki, T.; Crabtree, R. H. Homogeneous Tungsten, Rhenium, and Iridium Catalysts in Alkane Dehydrogenation Driven by Reflux of Substrate or of Cosolvent or by Inert-Gas Flow. *Organometallics* **1993**, *12*, 294−298.
(14) Zhu, K.; Achord, P. D.; Zhang, X.; Krogh-Jespersen, K.; Goldman, A. S. Highly Effective Pincer-Ligated Iridium Catalysts for Alkane Dehydrogenation. DFT Calculations of Relevant Thermodynamic, Kinetic, and Spectroscopic Properties. *J. Am. Chem. Soc.* **2004**, *126*, 13044−13053.
(15) Hartwig, J. F. *Organotransition Metal Chemistry*; University Science Books: Sausalito, CA, 2010.
(16) Weller, A. S.; Chadwick, F. M.; McKay, A. I. Transition Metal Alkane-Sigma Complexes. *Adv. Organomet. Chem.* **2016**, *66*, 223−276.
(17) Bergman, R. G. C−H Activation. *Nature* **2007**, *446*, 391.
(18) Zhu, Q.; Wang, G.; Liu, J.; Su, L.; Li, C. Effect of Sn on Isobutane Dehydrogenation Performance of Ni/SiO_2 Catalyst:

DOI: 10.1021/jacs.9b05577
J. Am. Chem. Soc. 2019, 141, 11700−11712

Adsorption Modes and Adsorption Energies of Isobutane and Isobutene. *ACS Appl. Mater. Interfaces* **2017**, *9*, 30711−30721.
(19) Calladine, J. A.; Duckett, S. B.; George, M. W.; Matthews, S. L.; Perutz, R. N.; Torres, O.; Vuong, K. Q. Manganese Alkane Complexes: An IR and NMR Spectroscopic Investigation. *J. Am. Chem. Soc.* **2011**, *133*, 2303−2310.
(20) Bernskoetter, W. H.; Schauer, C. K.; Goldberg, K. I.; Brookhart, M. Characterization of a Rhodium(I) -Methane Complex in Solution. *Science* **2009**, *326*, 553−556.
(21) Walter, M. D.; White, P. S.; Schauer, C. K.; Brookhart, M. Stability and Dynamic Processes in 16ve Iridium(III) Ethyl Hydride and Rhodium(I) σ−Ethane Complexes: Experimental and Computational Studies. *J. Am. Chem. Soc.* **2013**, *135*, 15933−15947.
(22) Yau, H. M.; McKay, A. I.; Hesse, H.; Xu, R.; He, M.; Holt, C. E.; Ball, G. E. Observation of Cationic Transition Metal-Alkane Complexes with Moderate Stability in Hydrofluorocarbon Solution. *J. Am. Chem. Soc.* **2016**, *138*, 281−288.
(23) Gonzalez, M. I.; Mason, J. A.; Bloch, E. D.; Teat, S. J.; Gagnon, K. J.; Morrison, G. Y.; Queen, W. L.; Long, J. R. Structural Characterization of Framework−Gas Interactions in the Metal−Organic Framework Co_2(Dobdc) by in Situ Single-Crystal X-Ray Diffraction. *Chem. Sci.* **2017**, *8*, 4387−4398.
(24) Asplund, M. C.; Snee, P. T.; Yeston, J. S.; Wilkens, M. J.; Payne, C. K.; Yang, H.; Kotz, K. T.; Frei, H.; Bergman, R. G.; Harris, C. B. Ultrafast UV Pump/IR Probe Studies of C−H Activation in Linear, Cyclic, and Aryl Hydrocarbons. *J. Am. Chem. Soc.* **2002**, *124*, 10605−10612.
(25) Guan, J.; Wriglesworth, A.; Sun, X. Z.; Brothers, E. N.; Zarić, S. D.; Evans, M. E.; Jones, W. D.; Towrie, M.; Hall, M. B.; George, M. W. Probing the Carbon−Hydrogen Activation of Alkanes Following Photolysis of Tp′Rh(CNR)(Carbodiimide): A Computational and Time-Resolved Infrared Spectroscopic Study. *J. Am. Chem. Soc.* **2018**, *140*, 1842−1854.
(26) Bengali, A. A.; Schultz, R. H.; Moore, C. B.; Bergman, R. G. Activation of the C-H Bonds in Neopentane and Neopentane-D_{12} by (η^5-$C_5(CH_3)_5$)Rh(CO)$_2$: Spectroscopic and Temporal Resolution of Rhodium-Krypton and Rhodium-Alkane Complex Intermediates. *J. Am. Chem. Soc.* **1994**, *116*, 9585−9589.
(27) Chen, G. S.; Labinger, J. A.; Bercaw, J. E. The Role of Alkane Coordination in C−H Bond Cleavage at a Pt(II) Center. *Proc. Natl. Acad. Sci. U. S. A.* **2007**, *104*, 6915−6920.
(28) Najafian, A.; Cundari, T. R. C−H Activation of Methane by Nickel−Methoxide Complexes: A Density Functional Theory Study. *Organometallics* **2018**, *37*, 3111−3121.
(29) McNamara, B. K.; Yeston, J. S.; Bergman, R. G.; Moore, C. B. The Effect of Alkane Structure on Rates of Photoinduced C−H Bond Activation by Cp*Rh(CO)$_2$ in Liquid Rare Gas Media: An Infrared Flash Kinetics Study. *J. Am. Chem. Soc.* **1999**, *121*, 6437−6443.
(30) Sattler, A. Hydrogen/Deuterium (H/D) Exchange Catalysis in Alkanes. *ACS Catal.* **2018**, *8*, 2296−2312.
(31) For intramolecular, agostic, sigma interactions alkyl dehydrogenation can be rather straightfoward. See, for example: Chaplin, A. B.; Poblador-Bahamonde, A. I.; Sparkes, H. A.; Howard, J. A. K.; Macgregor, S. A.; Weller, A. S. Alkyl dehydrogenation in a Rh(I) complex via an isolated agostic intermediate. *Chem. Commun.* **2009**, 244−246.
(32) Wasserman, E. P.; Moore, C. B.; Bergman, R. G. Gas-Phase Rates of Alkane C-H Oxidative Addition to a Transient CpRh(CO) Complex. *Science* **1992**, *255*, 315−318.
(33) Schultz, R. H.; Bengali, A. A.; Tauber, M. J.; Weiller, B. H.; Wasserman, E. P.; Kyle, K. R.; Moore, C. B.; Bergman, R. G. Ir Flash Kinetic Spectroscopy of C-H Bond Activation of Cyclohexane-D_0 and -D_{12} by Cp*Rh(CO)$_2$ in Liquid Rare Gases: Kinetics, Thermodynamics, and Unusual Isotope Effect. *J. Am. Chem. Soc.* **1994**, *116*, 7369−7377.
(34) Crestani, M. G.; Hickey, A. K.; Gao, X.; Pinter, B.; Cavaliere, V. N.; Ito, J.-I.; Chen, C.-H.; Mindiola, D. J. Room Temperature Dehydrogenation of Ethane, Propane, Linear Alkanes C4−C8, and Some Cyclic Alkanes by Titanium−Carbon Multiple Bonds. *J. Am. Chem. Soc.* **2013**, *135*, 14754−14767.
(35) Dobereiner, G. E.; Crabtree, R. H. Dehydrogenation as a Substrate-Activating Strategy in Homogeneous Transition-Metal Catalysis. *Chem. Rev.* **2010**, *110*, 681−703.
(36) Balcells, D.; Clot, E.; Eisenstein, O. C—H Bond Activation in Transition Metal Species from a Computational Perspective. *Chem. Rev.* **2010**, *110*, 749−823.
(37) Boutadla, Y.; Davies, D. L.; Macgregor, S. A.; Poblador-Bahamonde, A. I. Mechanisms of C−H Bond Activation: Rich Synergy between Computation and Experiment. *Dalton Trans.* **2009**, 5820−5831.
(38) Huang, Z.; White, P. S.; Brookhart, M. Ligand Exchanges and Selective Catalytic Hydrogenation in Molecular Single Crystals. *Nature* **2010**, *465*, 598−601.
(39) Petrosko, S. H.; Johnson, R.; White, H.; Mirkin, C. A. Nanoreactors: Small Spaces, Big Implications in Chemistry. *J. Am. Chem. Soc.* **2016**, *138*, 7443−7445.
(40) Pike, S. D.; Thompson, A. L.; Algarra, A. G.; Apperley, D. C.; Macgregor, S. A.; Weller, A. S. Synthesis and Characterization of a Rhodium(I) σ-Alkane Complex in the Solid State. *Science* **2012**, *337*, 1648−1651.
(41) Pike, S. D.; Chadwick, F. M.; Rees, N. H.; Scott, M. P.; Weller, A. S.; Krämer, T.; Macgregor, S. A. Solid-State Synthesis and Characterization of σ-Alkane Complexes, [Rh(L_2)(η^2,η^2-C_7H_{12})]-[$BAr^F{}_4$] (L_2 = Bidentate Chelating Phosphine). *J. Am. Chem. Soc.* **2015**, *137*, 820−833.
(42) Martínez-Martínez, A. J.; Tegner, B. E.; McKay, A. I.; Bukvic, A. J.; Rees, N. H.; Tizzard, G. J.; Coles, S. J.; Warren, M. R.; Macgregor, S. A.; Weller, A. S. Modulation of σ-Alkane Interactions in [Rh(L_2)(Alkane)]$^+$ Solid-State Molecular Organometallic (SMOM) Systems by Variation of the Chelating Phosphine and Alkane: Access to η^2,η^2-σ-Alkane Rh(I), η^2 σ-Alkane Rh(III) Complexes, and Alkane Encapsulation. *J. Am. Chem. Soc.* **2018**, *140*, 14958−14970.
(43) McKay, A. I.; Krämer, T.; Rees, N. H.; Thompson, A. L.; Christensen, K. E.; Macgregor, S. A.; Weller, A. S. Formation of a σ-Alkane Complex and a Molecular Rearrangement in the Solid-State: [Rh($CyP_2CH_2CH_2PCy_2$)(η^2,η^2-C_7H_{12})][$BAr^F{}_4$]. *Organometallics* **2017**, *36*, 22−25.
(44) Obenaus, F.; Droste, W.; Neumeister, J. In *Ullmann's Encyclopedia of Industrial Chemistry*; Wiley-VCH: Weinheim, 2014.
(45) Olah, G. A.; Molnár, Á.; Prakash, G. K. S. *Hydrocarbon Chemistry*; John Wiley & Sons, Inc: Hoboken, 2018.
(46) See Supporting Materials
(47) Chadwick, F. M.; McKay, A. I.; Martinez-Martinez, A. J.; Rees, N. H.; Krämer, T.; Macgregor, S. A.; Weller, A. S. Solid-State Molecular Organometallic Chemistry. Single-Crystal to Single-Crystal Reactivity and Catalysis with Light Hydrocarbon Substrates. *Chem. Sci.* **2017**, *8*, 6014−6029.
(48) Baumann, R.; Stumpf, R.; Davis, W. M.; Liang, L.-C.; Schrock, R. R. Titanium and Zirconium Complexes That Contain the Tridentate Diamido Ligands [(I-Pr^n-O-C_6H_4)$_2$]$^{2-}$ ([I-Prnon]$^{2-}$) and [(C_6H_{11}-O-C_6H_4)$_2$]$^{2-}$ ([Cynon]$^{2-}$). *J. Am. Chem. Soc.* **1999**, *121*, 7822−7836.
(49) Chapp, S. M.; Schley, N. D. Evidence for Reversible Cyclometalation in Alkane Dehydrogenation and C−O Bond Cleavage at Iridium Bis(Phosphine) Complexes. *Organometallics* **2017**, *36*, 4355−4358.
(50) See Supporting Materials for QTAIM, NBO and NCI plot data. A full account of the bonding in these and related alkane complexes will be the subject of a separate publication.
(51) Under these conditions an intermediate is observed on the way to [**1**-$BAr^F{}_4$], $\delta \sim 100$, that we have not been able to idenfity but propose it is the initial product of H_2-promoted alkane loss (see Figure S14).
(52) QTAIM, NBO and NCI analyses suggest an interaction intermediate between the extremes of η^2:η^2 and η^1:η^1 (see Figures S118−120 for details)

DOI: 10.1021/jacs.9b05577
J. Am. Chem. Soc. 2019, 141, 11700−11712

(53) Chadwick, F. M.; Rees, N. H.; Weller, A. S.; Krämer, T.; Iannuzzi, M.; Macgregor, S. A. A Rhodium−Pentane Sigma-Alkane Complex: Characterization in the Solid State by Experimental and Computational Techniques. *Angew. Chem., Int. Ed.* **2016**, *55*, 3677−3681.
(54) Characterized at low temperature by analogy with crystallographically characterized $[Rh(^{i}Pr_2PCH_2CH_2CH_2P^{i}Pr_2)(\kappa^2\text{-}Cl_2C_2H_4)][BAr^F{}_4]$. See ref 41.
(55) Douglas, T. M.; Chaplin, A. B.; Weller, A. S. Dihydrogen Loss from a 14-Electron Rhodium(III) Bis-Phosphine Dihydride to Give a Rhodium(I) Complex That Undergoes Oxidative Addition with Aryl Chlorides. *Organometallics* **2008**, *27*, 2918−2921.
(56) Chadwick, F. M.; Krämer, T.; Gutmann, T.; Rees, N. H.; Thompson, A. L.; Edwards, A. J.; Buntkowsky, G.; Macgregor, S. A.; Weller, A. S. Selective C−H Activation at a Molecular Rhodium Sigma-Alkane Complex by Solid/Gas Single-Crystal to Single-Crystal H/D Exchange. *J. Am. Chem. Soc.* **2016**, *138*, 13369−13378.
(57) *NMR Crystallography*; Harris, R. K., Wasylishen, R. E., Duer, M. J., Eds.; John Wiley & Sons: Chichester, 2009.
(58) Methylene groups C4 and C6 and each show one relatively close H···arene centroid distance 3.0 and 2.7 Å similar to $[\mathbf{1\text{-}NBA}][\mathbf{BAr^F{}_4}]$.
(59) Smart, K. A.; Grellier, M.; Coppel, Y.; Vendier, L.; Mason, S. A.; Capelli, S. C.; Albinati, A.; Montiel-Palma, V.; Muñoz-Hernández, M. A.; Sabo-Etienne, S. Nature of Si−H Interactions in a Series of Ruthenium Silazane Complexes Using Multinuclear Solid-State NMR and Neutron Diffraction. *Inorg. Chem.* **2014**, *53*, 1156−1165.
(60) Lawes, D. J.; Darwish, T. A.; Clark, T.; Harper, J. B.; Ball, G. E. A Rhenium−Cyclohexane Complex with Preferential Binding of Axial C−H Bonds: A Probe into the Relative Ability of C−H, C−D, and C−C Bonds as Hyperconjugative Electron Donors? *Angew. Chem., Int. Ed.* **2006**, *45*, 4486−4490.
(61) Torres, O.; Calladine, J. A.; Duckett, S. B.; George, M. W.; Perutz, R. N. Detection of σ-Alkane Complexes of Manganese by NMR and IR Spectroscopy in Solution: $(\eta^5\text{-}C_5H_5)Mn(CO)$ (Ethane) and $(\eta^5\text{-}C_5H_5)Mn(CO)$(Isopentane). *Chem. Sci.* **2015**, *6*, 418−424.
(62) Pitts, A. L.; Wriglesworth, A.; Sun, X.-Z.; Calladine, J. A.; Zarić, S. D.; George, M. W.; Hall, M. B. Carbon−Hydrogen Activation of Cycloalkanes by Cyclopentadienylcarbonylrhodium—a Lifetime Enigma. *J. Am. Chem. Soc.* **2014**, *136*, 8614−8625.
(63) Addition of D_2 to $[\mathbf{1\text{-}C_4H_{10}}][\mathbf{BAr^F{}_4}]$ does, however, result in D-incorporation into both methine and methyl groups.
(64) Perutz, R. N.; Sabo-Etienne, S. The σ-CAM Mechanism: σ Complexes as the Basis of σ-Bond Metathesis at Late-Transition-Metal Centers. *Angew. Chem., Int. Ed.* **2007**, *46*, 2578−2592.
(65) Hoops, S.; Sahle, S.; Gauges, R.; Lee, C.; Pahle, J.; Simus, N.; Singhal, M.; Xu, L.; Mendes, P.; Kummer, U. Copasi—a Complex Pathway Simulator. *Bioinformatics* **2006**, *22*, 3067−3074.
(66) Oliván, M.; Marchenko, A. V.; Coalter, J. N.; Caulton, K. G. Gas/Solid Reactivity of Unsaturated Ruthenium-Containing Molecular Solids. *J. Am. Chem. Soc.* **1997**, *119*, 8389−8390.
(67) Albrecht, M.; Lutz, M.; Schreurs, A. M. M.; Lutz, E. T. H.; Spek, A. L.; van Koten, G. Self-Assembled Organoplatinum(II) Supermolecules as Crystalline, SO_2 Gas-Triggered Switches. *J. Chem. Soc., Dalton Trans.* **2000**, 3797−3804.
(68) Albrecht, M.; Lutz, M.; Spek, A. L.; van Koten, G. Organoplatinum Crystals for Gas-Triggered Switches. *Nature* **2000**, *406*, 970−974.
(69) A consecutive second-/first-order process also fits the data, but less well than two first-order processes. However, given the lack of data points that define the first dehydrogenation we cannot rule out this possibility.
(70) Sadow, A. D.; Tilley, T. D. Homogeneous Catalysis with Methane. A Strategy for the Hydromethylation of Olefins Based on the Nondegenerate Exchange of Alkyl Groups and σ-Bond Metathesis at Scandium. *J. Am. Chem. Soc.* **2003**, *125*, 7971−7977.
(71) Bertmer, M.; Nieuwendaal, R. C.; Barnes, A. B.; Hayes, S. E. Solid-State Photodimerization Kinetics of A-Trans-Cinnamic Acid to A-Truxillic Acid Studied Via Solid-State NMR. *J. Phys. Chem. B* **2006**, *110*, 6270−6273.
(72) Hulbert, S. F. Models for Solid-State Reactions in Powdered Compacts: A Review. *J. Br. Ceram. Soc.* **1969**, *6*, 11−20.
(73) Finney, E. E.; Finke, R. G. Is There a Minimal Chemical Mechanism Underlying Classical Avrami-Erofe'ev Treatments of Phase-Transformation Kinetic Data? *Chem. Mater.* **2009**, *21*, 4692−4705.
(74) Khawam, A.; Flanagan, D. R. Solid-State Kinetic Models: Basics and Mathematical Fundamentals. *J. Phys. Chem. B* **2006**, *110*, 17315−17328.
(75) Benedict, J. B.; Coppens, P. Kinetics of the Single-Crystal to Single-Crystal Two-Photon Photodimerization of A-Trans-Cinnamic Acid to A-Truxillic Acid. *J. Phys. Chem. A* **2009**, *113*, 3116−3120.
(76) Jarvis, A. G.; Sparkes, H. A.; Tallentire, S. E.; Hatcher, L. E.; Warren, M. R.; Raithby, P. R.; Allan, D. R.; Whitwood, A. C.; Cockett, M. C. R.; Duckett, S. B.; Clark, J. L.; Fairlamb, I. J. S. Photochemical-Mediated Solid-State [2 + 2]-Cycloaddition Reactions of an Unsymmetrical Dibenzylidene Acetone (Monothiophos-Dba). *CrystEngComm* **2012**, *14*, 5564−5571.
(77) Hatcher, L. E.; Skelton, J. M.; Warren, M. R.; Stubbs, C.; da Silva, E. L.; Raithby, P. R. Monitoring Photo-Induced Population Dynamics in Metastable Linkage Isomer Crystals: A Crystallographic Kinetic Study of $[Pd(Bu_4dien)NO_2]BPh_4$. *Phys. Chem. Chem. Phys.* **2018**, *20*, 5874−5886.
(78) Pike, S. D.; Krämer, T.; Rees, N. H.; Macgregor, S. A.; Weller, A. S. Stoichiometric and Catalytic Solid−Gas Reactivity of Rhodium Bis-Phosphine Complexes. *Organometallics* **2015**, *34*, 1487−1497.
(79) Under this constraint there are two structures that can be generated depending on which C−C is dehydrogenated. The more stable option is used here, and details of the alternative structure are provided in the Supporting Information.
(80) The alternative pathway based on initial $C-H^3$ bond activation has a slightly larger barrier of 23.9 kcal/mol and is generally somewhat less accessible than the pathway in Figure 7. This reflects the asymmetry of the cyclohexane binding pocket which renders the $C-H^1$ and $C-H^3$ bonds inequivalent. Full details of this alternative pathway are in the Supporting Information.
(81) A geometry for **VI** in which H_2 was retained in the lattice was also derived from the characterisation of **TS(V-VIa)**. This had a free energy of +9.7 kcal/mol and had essentially the same coordination geometry around Rh. The drop in free energy to +2.8 kcal/mol reflects the entropy gain upon releasing free gaseous H_2. See Supporting Information for details, Figure S101.
(82) This value differs from ΔG^{Rh} (+6.3 kcal/mol) as the two models employed are not the same: here one Rh-cyclohexene moiety is computed in the presence of three Rh-cyclohexane cations (and four $[BAr^F{}_4]^-$ anions), whereas ΔG^{Rh} is based on dehydrogenation of all four Rh centers.
(83) An alternative pathway based on the initial formation of an *endo*-Rh−H/allyl intermediate, a trans−cis isomerisation prior to H_2 loss was ruled out on the basis of calculations on the isolated cation that indicated a high energy isomerisation process. See Supporting Information for details, Figure S100.
(84) A related transition state at +16.5 kcal/mol involves counter-clockwise rotation of the cyclohexane and generates a 2,6-structure that is geometrically equivalent to the initial 1,3-chair (Supporting Information, Figure S107).
(85) Kumar, A.; Zhou, T.; Emge, T. J.; Mironov, O.; Saxton, R. J.; Krogh-Jespersen, K.; Goldman, A. S. Dehydrogenation of N-Alkanes by Solid-Phase Molecular Pincer-Iridium Catalysts. High Yields of A-Olefin Product. *J. Am. Chem. Soc.* **2015**, *137*, 9894−9911.
(86) Sheludko, B.; Cunningham, M. T.; Goldman, A. S.; Celik, F. E. Continuous-Flow Alkane Dehydrogenation by Supported Pincer-Ligated Iridium Catalysts at Elevated Temperatures. *ACS Catal.* **2018**, *8*, 7828−7841.

DOI: 10.1021/jacs.9b05577
J. Am. Chem. Soc. 2019, 141, 11700−11712